JONAS

Joint Framework for Ocean Noise in the Atlantic Seas

EAPA_52/2018

A 5.3 Calibrate / ground truth using acoustic data provided by WP4

D5.3 : Standards for the calibration of acoustic modeling

	Reference	Issue	Dissemination status
Deliverable	D5.3		
File name	*JONAS_5.3*		

Author(s)	*Organisation*	*Version and Date*	*Author(s)*
David Dellong, Florent Le Courtois	SHOM, Brest, France		
Ricardo Duarte, Sérgio M. Jesus	LARSyS, University of Algarve, Faro, Portugal		
Checked by			
Approved by			

EXECUTIVE SUMMARY

Jonas will develop and pilot a noise-monitoring platform, harmonize technical approaches to MSFD requirements, and promote the adoption of quieter operational practices among users of the NE Atlantic marine space.

This effort will essentially be based on extensive computer modeling using AIS and archival environmental data to achieve the necessary coverage for the wide Atlantic area. Although the collection of actual field data is not foreseen during the project itself, devising methods for calibrating model output to better represent the reality is an absolute requirement. That is why work package 5 deals with methodologies for computing noise maps and encompasses a task dedicated to model calibration through ground truth acoustic measurements, under which this work was performed.

Ground truth calibration, here after "field calibration", represents a challenge for at least two main reasons: one, is that the number of field observations are in all circumstances too few for efficiently constrain the modeled field in large areas and during long periods of time, and second, there is no known way to validate the calibrated field in a way to direct the calibration effort. In practice, there is no well accepted methodology for field calibration and/or for data sampling strategy. Efforts in that direction in previous EU projects such as BIAS and JOMOPANS provided data model comparisons but no definite calibration strategies, entailing model modification to approach the observed data.

This report summarizes the work performed under the task dedicated to field calibration where the problem is analyzed by describing previously proposed techniques and a number of possible future approaches with their advantages and drawbacks are outlined. One of those approaches to our knowledge, not previously tested on real data, was implemented in a data set kindly provided to JONAS by the IMAR Okeanos group of the Azores University, with interesting results. Data - model comparisons is then performed through objective distribution distance indicators and tested in another data set gathered in the southwest approaches to the channel, off Bretagne.

Future developments will encompass the usage of this and other field calibration techniques for computing broadband continuous noise and cetaceans impact indicators. Journal and conference publications of this work are being submitted.

Table of Contents

1. Introduction

When the focus is random ocean sound, there is no particular signal to detect or to estimate so, the interest is on the sound structure and on the noise "amount", *i.e.*, its intensity, classically defined as the sound pressure level (SPL), evaluated at any moment in time, space and frequency. Sound structure relates to its correlation in time and/or space and eventual directionality. Often, the main goal is to be able to estimate SPL everywhere with a limited number of observations, which is a rather ill-posed task.

There is an ongoing research topic in the underwater noise community regarding the question of "What is the ocean sound reference level?", or, in other words, "how did the ocean sound like many years ago, before the industrial revolution?". The assumption behind this question is that the sound level in the ocean should have been constant throughout the centuries, and should have started to change only when coal burning steam ships started to cross the oceans, in the early 19th century. Fishing and recreational vessels, although more geographically localized, also suffered a steep increase in the last 2/3 decades. The economic process of globalization contributed to a dramatic increase in ship traffic and therefore to ocean noise [1]. Early ocean sound measurements suffered from a lack of measurement equipment with both the endurance and low (self-)noise required for reliable ocean noise measurements.

Noise mapping is performed in order to investigate the continuous noise generated by anthropogenic activities and estimate its contribution to the ambient noise of the North-East Atlantic Ocean. As part of the EU Marine Strategy Framework Directive (MSFD [41]), these noise maps are envisaged to monitor and assess the underwater continuous noise levels and their threat to marine ecosystems.

Model validation is the process that aims to include information from acoustic measurements recorded at sea into the results from the models directly or into the models themselves. This process is organized in several steps that are described in Figure 1.1. The comparison and the calibration are key steps. Comparison is often performed by investigating the statistical differences of the noise level distributions over time between models and measurements at the recording position (e.g. using Cumulative Density Function in the BIAS project [27]). The calibration relies on this information to adjust different parameters or the models themselves in order to fit the computed noise level distributions to the measurements.

Several projects have already produced noise maps that include a validation process. For example in the EU, the Baltic seas were studied by the BIAS project, and the North Sea by the JOMOPANS project. These areas share a common environmental setting that is a mostly shallow water environment. In this framework and for low frequencies, the seabed properties are expected to have a strong influence on the received levels. Hence, in the BIAS project, the calibration process involved adjusting the bottom properties locally. The vessel source levels were also adjusted locally according to the measurements. Similar requirements were proposed in the QuietMEd project (Deliverable D3.3 of this project [37]). The goal was to perform acoustic data assimilation.

Noise maps in the JOMOPANS project were not calibrated using at sea measurements directly, as it was performed in BIAS. The final noise maps were produced using three optimizations of the semi-empirical models: the ship source levels model (following ECHO programme), the seafloor geo-acoustic model (Zhou et al, 2009 [42]) and the wind noise model (Ainslie et al, 2011).

In the JONAS project, because of the area covered, it was not possible to perform calibration of the noise maps. In this document, the comparisons between measured and simulated noise levels are performed in order to provide confidence maps. The methodology is explained and two case studies are provided in the annexes.

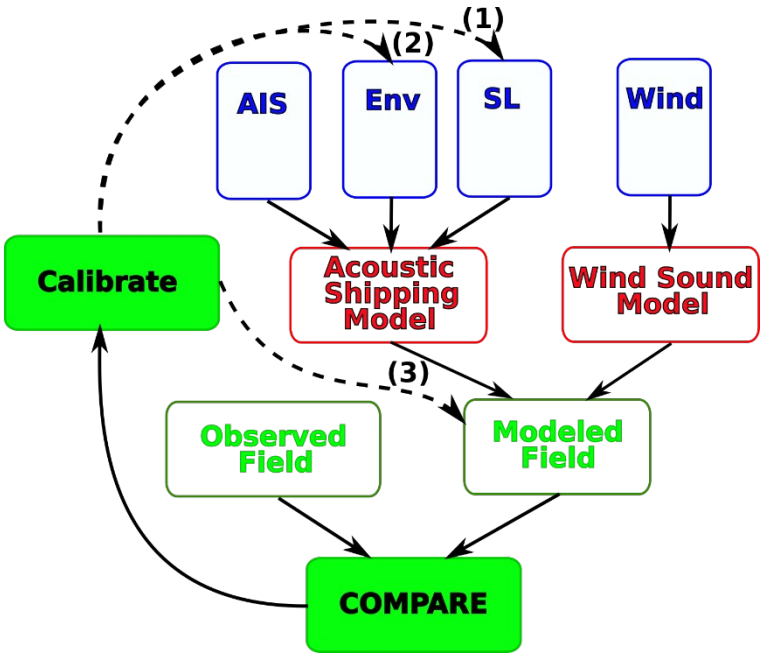

Figure 1.1: Sound model calibration through the integration of observations.

2. Ocean sound models

2.1. Shipping noise models

In the JONAS project, the shipping noise maps (Figure 2.1) at coarse resolution were produced following the methodology detailed in the JONAS deliverable 5.2 and [28]. From the passive SONAR equation, the received levels are modeled by subtracting the source levels (SL) by their associated transmission losses (TL). Both are computed separately and relies on numerous non-acoustic data that define the propagation environment and the local shipping activity.

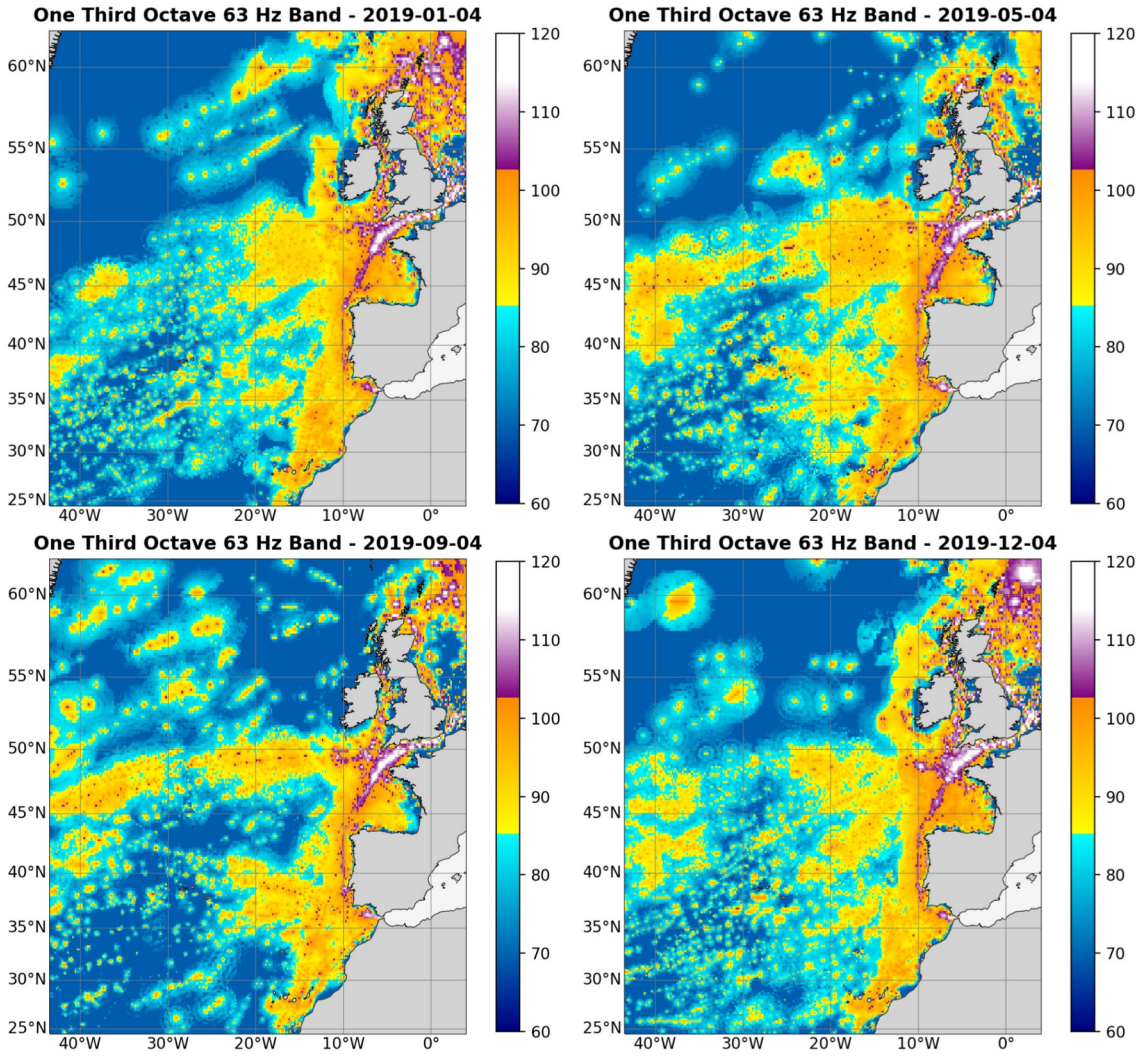

Figure 2.1: Example of the results obtained for the large-scale JONAS area, for four days of different months. The daily shipping noise maps are produced for the 1/3-octave band centered on 63 Hz. Scales are in decibels reference 1 µPa.

2.2. Wind sound modeling

Sound generated at the sea surface by the action of wind and induced waves is known to be predominant above a frequency of a few hundred Hz [2]-[4]. Below that frequency wind sound exists but is overcome by the noise due to distant shipping (30-150 Hz) and/or earthquakes (< 30 Hz). So, the observation of wind driven sound between a few tens of Hz and a few hundred Hz is contaminated by shipping noise, especially in the northern hemisphere where it is difficult to perform experimental measurements in shipping noise free areas. The contribution of Cato [5] with ocean sound measurements in Australian waters where shipping noise is low, and later by Burgess [6] using a surface steered vertical array to exclude shipping noise from distant sources, was determinant for establishing an empirical dependence of ocean sound on frequency and wind speed on one hand [6], [7] and on surface wind sound levels, on the other hand [7], [8].

So, there are mainly two approaches: in the first one it is acknowledged that wind sound depends only on wind speed and frequency and it attempts to fit observed sound with these

two parameters. The other, models wind sound as that produced by a uniform infinite sheet of sound sources near the surface and then propagates the sound generated by those sources to the observation position, using the local conditions (bathymetry, sound speed, etc) [8]. In the example of the Azores, treated below (section 6-b), we will be adopting the first approach.

So, in the first approach a suitable distribution may be obtained by considering that proposed by Kewley *et al.* [7], that assumes the underlying process of surface wind sound generation as having two mechanisms: one for low sea state and another for high sea state, involving white caps. The separation of the two mechanisms is roughly between 8 and 10 knots. According to this assumption a possible curve fitting is to allow two slopes for the wind speed dependency so that sound intensity could be written as:

$$p^2(f)=av+b\,v^3,$$

and the sound spectrum level NL in dB to be given by:

$$NL(f,v)=10\log_{10}\left[10^{L_1(f,v)/10}+10^{L_2(f,v)/10}\right],$$

where the two terms L_1 and L_2 are given by:

$$L_1(f,v)=A(f)+10\log_{10}v,$$

$$L_2(f,v)=B(f)+30\log_{10}v,$$

where $A(f)=10\log_{10}(a)$ and $B(f)=10\log_{10}(b)$. Kewley *et al.* [7] does not give the curve fitting coefficients a and b so it is necessary to resort to the estimated source level spectra shown in Fig. 3 of [7], which requires adding bottom loss. According to Fig. 11 of [6], the frequency dependency of bottom loss may be approximated by a straight line of the form:

$$BL(f)=0.0073f+0.731,$$

with f in Hz and BL in dB. Using (3) one can get the sound level correction factor $C(f)$ (see eq. 7 of [6]) as:

$$C(f)=10\log_{10}\left[\frac{b(f)+1}{b(f)-1}\right],$$

where $b(f)=10^{BL(f)/10}$. For reference, bottom loss frequency dependence is shown in Fig. 1(a) and the $C(f)$ factor is shown in (b). These two figures basically say that bottom loss increases with frequency and that the correction factor is as small as energy remains trapped in the bottom with bottom loss increase.

(a) (b)

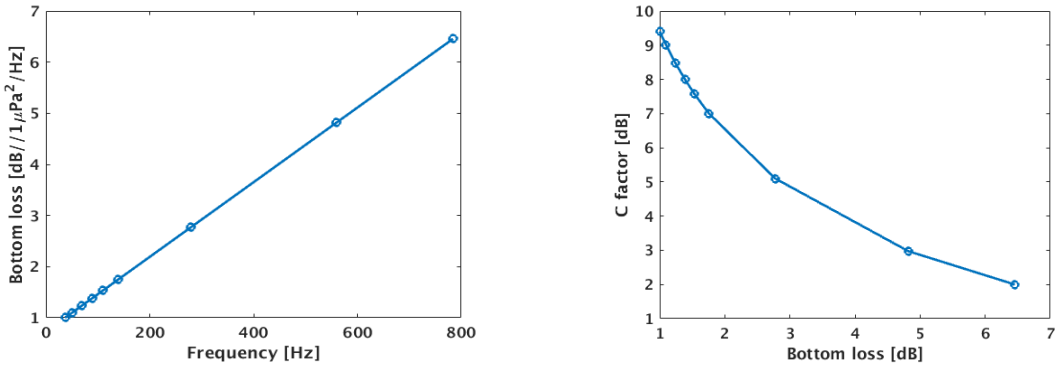

Figure 2.2: Bottom loss effect as suggested by Burgess and Kewley [6]: bottom loss frequency dependence (a) and sound level factor as given by (4) (b).

Using $C(f)$ and the source level SL of Fig. 3 of [7] into:

$$NL(f,v)=SL(f,v)+C(f)+8,$$

one gets the sound spectrum level in dB//1μPa^2/Hz. Figure 2.3 shows source level as per Fig. 3 of [7] (a) and calculated sound spectrum level given by (5) in (b).

(a) (b)

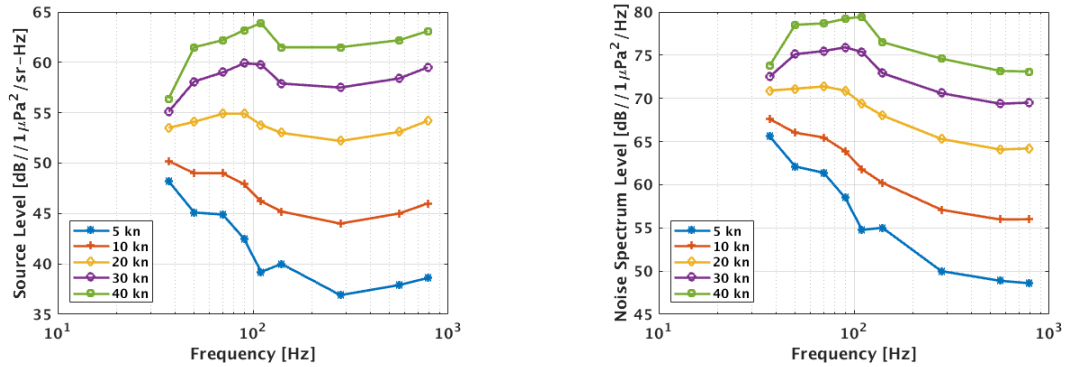

Figure 2.3: Kewley et al. [7] empirical wind sound model: source level (a) noise spectrum level (b), for various wind speeds.

In order to be able to generate the wind sound level for any wind speed a nonlinear curve least squares fitting was performed for coefficients $A(f)$ and $B(f)$ generating the approximate curves as shown in Fig. 3 for wind speed (a) and for sound level (b).

(a) (b)

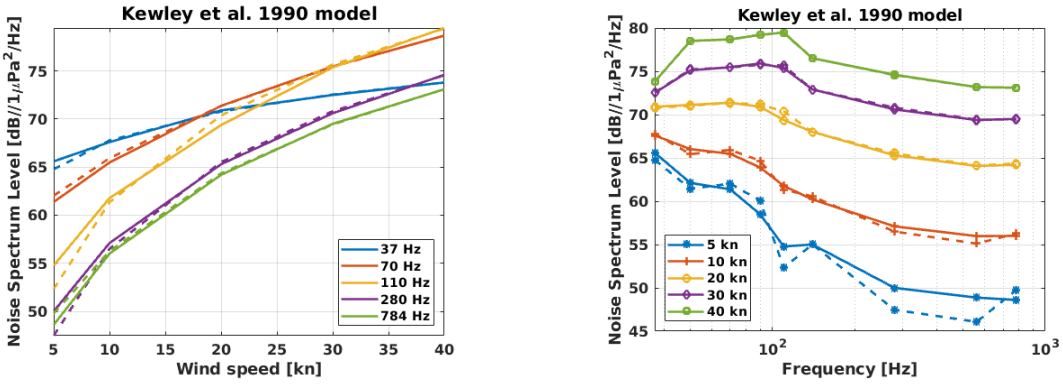

Figure 2.4: Kewley et al. [7] empirical wind sound model nonlinear least squares fitting: for wind speed (a) and for noise spectrum level (b).

It is clear that the approximation error is smaller at higher wind speeds.

3. Modeling errors

Noise maps are uncertain because of errors and uncertainties. Figure 3.1 highlights dependencies among data used in modeling (see DL5.1) on the noise level assessment. In the following, errors are discussed whether they could be attributed to the source level or the propagation model. These two processes are generally distinct and have differentiated impacts.

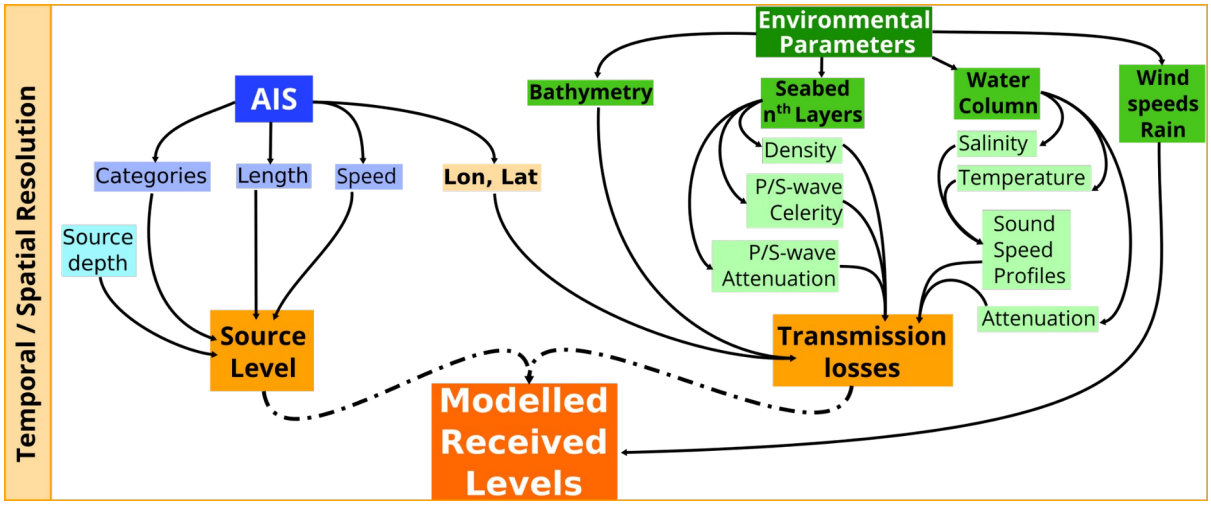

Figure 3.1: Underwater acoustic modeling and non-acoustic data dependencies.

3.1. Source level error

Source level usually refers to the equivalent noise generated by a ship at a single point at 1 m distance from this point. This approximation might be strongly unrealistic for very large ships. In order to model the source level (SL) radiated from a position (defined by AIS data) different source models are commonly adopted for their ease of use *(Ross and Kuperman, 1989 [29]; Breeding et al., 1996 [30]; Wagstaff, 1973 [31]; Wales and Heitmeyer, 2002 [32]; Audoly and Rizzuto, 2015 [33]; Audoly et al. 2015 [34]; Wittekind, 2014 [35])*. No consensus has been found on the source model but most recent noise mapping projects are using RANDI 3.1 model (*Breeding et al., 1996 [30]*) as it can be implemented easily and requires vessel information that are commonly provided in AIS catalogs.

The origin of errors on the source level modeling are summarized here:

- The single source point approximation.
- The source model itself.
- From the AIS data feeding the model:
    - Missing, or wrong vessel information in the AIS catalog.
    - AIS data comprehensiveness, such as data gaps (spatial, temporal resolution, duplicated position or missing vessels). This is a commonly encountered issue as not all vessels are using AIS transceivers.

To alleviate these issues and possible errors, the source level modeling can rely on several:

- AIS data interpolation of the positions
- Vessel classification using different vessel categories with unique source model for each.
- Production of statistical products, such as vessel density maps.

These solutions were used in the JONAS noise mapping process (see deliverable D5.2), but the source model itself is very difficult to modify and generalize. Several EU projects already explored this option and they proposed updates to the source models that rely on more or less vessel parameters and categories *(e.g. AQUO project [33, 34, 39])*.

3.2. Transmission loss error

The Transmission Loss (TL) computation requires an accurate description of environment physical properties, in order to model the acoustic propagation. This modeling phase relies on the usage of environmental data that are listed in the deliverable D5.1 (Bathymetry, sound speed profiles (SSP) and seabed properties). The TL computation related issues are listed here:

- Source and receiver depth locations
- Model-related errors:
    - unadapted model usage and wrong approximation (e.g. ray-based method at low frequency);
    - numerical errors and artifacts;
    - 3D effects of the environment that are not considered;
    - computation time-related approximations (e.g. limited maximum distance between source and receiver).

- Environmental data related errors:
  - data gaps;
  - errors in the input data;
  - inappropriate spatial and temporal resolutions.

3.3. Model parameterization

Temporal and spatial resolutions are defined by users and follow scientific / regulatory needs. This decision is defined by expert judgment and is mostly motivated by computation efficiency, as large areas and/or fine resolution maps are difficult to model in reasonable computation time. The resolution dependency is an important parameter, especially for model/measure comparison purposes, and the relationship between different resolutions needs further investigation.

4. Comparison to measurements

4.1. Acoustic data

Acoustic data used in the JONAS project were opportunistic datasets provided by project partners. A list of available datasets is given with details in the JONAS deliverable 4.1. Therefore, the contributing acoustics projects may not have been designed in the most optimal way for the purpose of validation and uncertainty assessment. Measurement data were processed by the partners in order to provide the Sound Pressure Level (SPL) for both the 63, and 125 Hz One Third Octave (OTO) bands.

4.2. modeled noise map

The resulting noise maps used for the comparison are the preliminary noise maps (JONAS deliverable 5.2) modeled at 63, and 125 Hz OTO bands.

4.3. Noise level comparison

The noise level estimation over a time period from the measurements and the modeled noise maps allow estimating the frequency of occurrence of several bins of acoustic levels by building an histogram. The Probability Density Function (PDF) is built by normalizing the distribution of temporal occurrences in one cell of the map. The temporal PDF allows the comparison of values of density between the two datasets.

Other studies generally consider a direct comparison of the distribution by using statistical moments like mean, median and standard deviation (SD). A set of percentiles can be chosen to compare the distributions in a more detailed analysis (JOMOPANS project in Putland et al., 2021 report [36] and [40]). In the BIAS project the comparison was carried out by using cumulative density functions (CDF) from the temporal distribution of noise levels (Folegot et al., 2016 *[27]*).

4.4. Distances between distributions

Quantifying distances between probability density functions is a recurrent problem explored through different concepts in the evidence theory (Jousselme et al., 2012 [36]). The distances used in this study were chosen from a long list of distances defined in (Cha, 2007 [44]). Four different methods were used to compare the measured and modeled noise levels distribution over the same period of time. These distances are proposed as supplementary information adding to the commonly used statistical moments of the distributions. The distance values could allow modelers to obtain more information and orient the calibration step. Moreover, such values could help automatize the comparison process for several recording stations and also ease the comparison between distant recorders.

4.4.1. Statistical moments

Mean, median and SD are computed to assess relevant information about the distributions. These values are directly in dB which ease their interpretation. These common values and percentiles are commonly compared in most projects. Comparing these values is straightforward, and simple differences between medians or means has been commonly used to validate models.

In the following, for a number of d bins, P_i and Q_i are the probability of the i^{th} bin for the measurements and the model data respectively.

4.4.2. Minkowski distance

Minkowski distance is defined in (6). It is a measure of the distance between the probabilities for each bin. It can be interpreted as a rough estimation of the distance between the complete distributions. This is performed in a similar way as comparing the statistical moments, or the percentiles, which return a distance between distributions considering each bin.

$$d_{mk} = \sqrt[p]{\sum_{i=1}^{d} \left| P_i - Q_i \right|^p} \tag{6}$$

Minkowski distance formulation, between Q and P, two PDFs which are computed from histograms over a total of d bins. The norm is denoted by p, when p=2 as performed in this study, the Euclidean distance is computed.

4.4.3. Sørensen / Czekanowski

Sørensen / Czekanowski similarity as defined in (7), can be interpreted as how much overlap is observed between the distributions.

$$d_{sor} = \frac{\sum_{i=1}^{d} \left| P_i - Q_i \right|}{\sum_{i=1}^{d} (P_i + Q_i)} \tag{7}$$

Sørensen / Czekanowski distance formulation. The Sørensen similarity is used in this document and is defined as 1 - dsor.

4.4.4. Normalized Sørensen / Czekanowski similarity

A normalization to the mean or the median of the measured and modeled noise values before computing the histogram and distributions can be performed in order to recenter the distributions. A second step is performed to quantify the similarity of the shape of the normalized distributions by re-using the Sørensen / Czekanowski defined in (7).

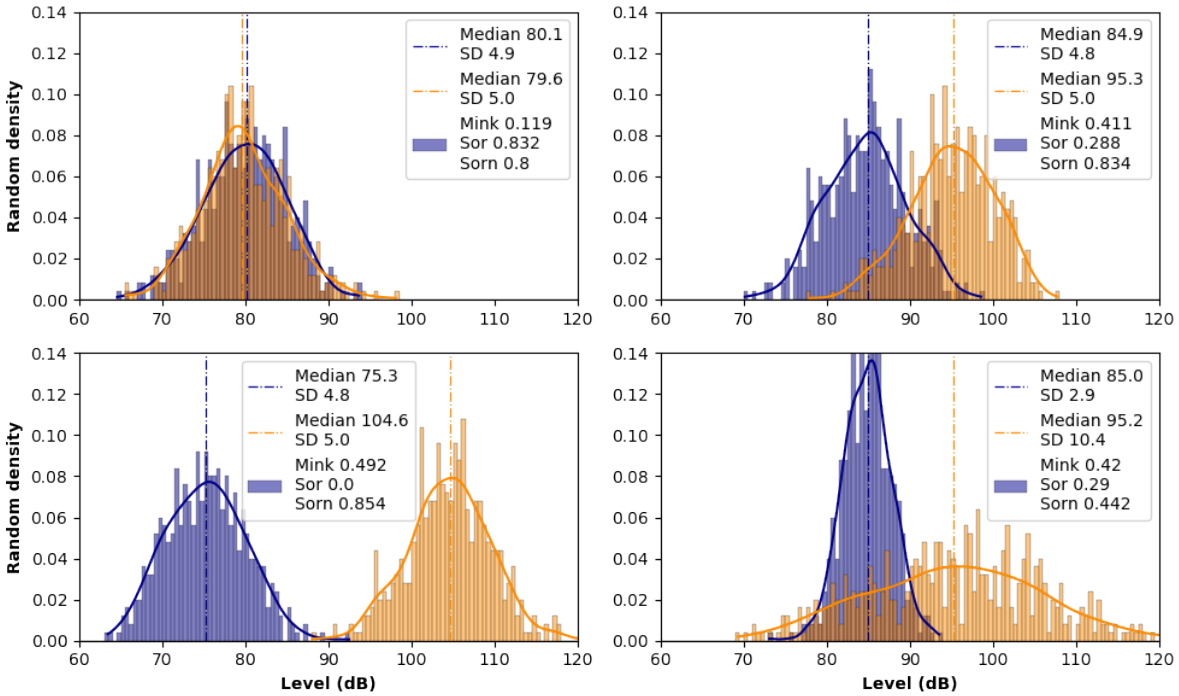

Figure 4.1: Randomly generated normal distributions and the associated distances between them. Distances are computed using the methods described above. SD: Standard Deviation; Mink: Minkowski distance; Sor: Sørensen / Czekanowski similarity; Sorn: Normalized distributions to the median and Sørensen / Czekanowski similarity.

4.5. Spatial extent of the comparison

The statistical noise maps modeled by following the methodology described in JONAS D5.2 are producing uncertain results. Using the distances and comparison presented above, uncertainty can be attributed to models at these specific locations and time periods. As multiplying the number of measurements is not always possible, providing validated and error estimation over a large area is not possible. This problem could be tackled by extending the local uncertainties further away from the recorders. The goal is to define a spatial neighborhood in which the comparison between model and measurements can be extended, whether it concerns match or mismatch. For this purpose, we introduce the confidence area, that could be simplified as a confidence radius around the recorder position in idealistic cases. Therefore, we assumed that model mismatch, assessed when comparing the distribution, is of the same magnitude in the confidence area (or defined by the range in the confidence radius).

The confidence radius computation is based on propagation range, above which the acoustic contribution at the receiver can be neglected. A threshold of 100 dB attenuation of the emitter source level is set. Thus, the radius defines the median range of propagation of a signal of 100 dB around the recorder. This definition does not consider other sources' contribution and local noise at the receiver position, as it would have been taken into account in classical detection performance.

The method used to determine the confidence radius is presented here:

- Compute TL from the recorder position in 8 directions.
- Find the distance above which the TL value is too big to consider significant contribution of the source without noise (e.g. 100 dB at 63 Hz).
- The confidence radius is the median distance for a source to have a significant contribution

This definition is strongly empirical, and depends on several parameters like the frequency.

5. Data fitting or field calibration

Assimilation of acoustic measurements can be defined as a more advanced process. It aims at integrating measurements into model output. Such a process has not been strongly investigated yet in underwater acoustics as it requires a dense network of acoustic recordings. However, the amount of measurements required is too limited to apply such methodologies to underwater acoustics in a straightforward way.

The correction of underwater noise maps is commonly performed using local or global geoacoustic inversion of the environment. Usually, geoacoustic inversion is performed by minimizing error between measured and simulated physical quantities: mode arrivals, angles...; inversion for noise maps considered mainly on matching acoustics levels.

The global error is often related to a complex interaction between parameters listed in Section 3. Depending on the frequency, different physical properties can be identified as the main contributor to the error. At low frequencies, the seabed acoustic properties were identified as the main contributors to error as it remains poorly known and difficult to estimate. Two main inversion methods have been proposed to correct sound speed and sediment absorption. The method must guarantee that inverted parameters respect physical properties. The spatial extent of the validation must be considered as well, and the correction may not be generalized to larger areas.

In theory the data fitting problem may be formulated as follows:

Given the noise observation data set O, estimate the set of parameters θ_N such that:

$$\hat{\theta}_N = \min_{\theta} J\left(N(\theta), O\right)$$

where $N(\theta)$ is our sound model output for input parameter θ, and $J(\cdot)$ is some cost function adjusting the model to the observations.

This process, known as “field calibration”, may be schematically represented by the diagram of Fig. 1.1 where it is assumed, in a first approximation, that for the considered frequency band: the anthropogenic noise component is reduced to shipping noise; the abiotic noise is dominated by surface wind generated sound, and the biotic component is too sparse in time and space to be considered for continuous sound measurements.

The correction of underwater noise maps is commonly performed using local or global geoacoustic inversion of the environment. Usually, geoacoustic inversion is performed by minimizing error between measured and simulated physical quantities: mode arrivals, angles...; inversion for noise maps considered mainly on matching acoustics levels.

The expectation is that parameter vector $\hat{\theta}_N$ resulting from minimization (8), will procure a better model to data adjustment even outside the time, frequency and, especially, spatial window of the observations than the forward model $N(\theta_N^{¿})$ for some basic default a priori parameter vector $\theta_N^{¿}$.

Comparison is obviously performed only for the current time-frequency-space data cube where observations are being carried out and may take various forms, depending on the optimization strategy being sought. There are, at least, three alternatives for model calibration:

1. **environmental focusing** which proceeds by changing environmental parameters at the input of the acoustic propagation model (ENV box marked as (1) in Fig. 1.1) is similar to the ill-posed problem of environmental parameter estimation faced for example in popular matched-field techniques, such as MFP, OAT or MFI (see below for references). It normally entails an optimization procedure that “navigates” in a very large multidimensional parameter space, making it possibly even more ill-posed than MFP;

2. **source level adjustment** that estimates ships’ source level intensity (SL box marked as (2) in Fig. 1.1), requires determining the level of excitation of every sound source within receivers’ acoustic reach, and then expecting that those ships will cross the area maintaining that level of emission, in order to better constrain the sound map over time and space. The process may be quite challenging and hangs on several assumptions;

3. **direct model transformation** for the calibration process to directly apply feedback of the data - model match on the acoustic model or wind model outputs (marked as (3) in Fig. 1.1). This may be performed by determining field weights from data-model statistical distributions and wisely use those weights to calibrate model outputs;

Of course, the options above do not exclude the possibility of combining two or more of these alternatives, which may procure a more realistic and possibly better adjustment at the expense of a higher computational burden.

5.1. Environmental focusing

Parameter adaptation may take advantage of a large body of work on ocean environmental parameter estimation using underwater acoustics, generically called as matched-field (MF) based methods. Those methods are rooted in the seminal work of Hinich

[9] and Bucker [10] then popularized as matched-field processing (MFP - see [11], [12] for reviews), initially proposed for acoustic source localization. The turning point from MFP to environmental parameter estimation started with the work of Collins [13] on MF focalization, where the environmental parameters are adjusted until the source position turns into focus. Some authors separate environmental estimation MF methods for water column properties, as ocean acoustic tomography (OAT) [14]-[16], from bottom parameter estimation, known as matched-field inversion (MFI) [17]. In some cases, the objective was to obtain the source location without knowing the media environmental parameters (this is normally called blind source localization) [18]. The inversion process relies on the uniqueness of the acoustic observation relative to the parameters to be estimated. That uniqueness depends on the frequency band being used, on the temporal and spatial span of the observations and, of course, on the particular propagation conditions. In most MF application examples found in the literature the field is assumed to be illuminated by a single source.

In the sound mapping case, sources are multiple and their location is known (AIS information is required). So, the objective becomes that of fitting the model output to the data, constrained to a given SPL at the Q_t source location. This objective may be expressed as:

$$J_{mf}(\theta)=\min_{\theta} \| o-m(\theta) \|^2 s.t.\{m_q(\theta)=s_q, q=1,\ldots,Q_t\},$$

where o are the observations, m is the model output (it includes both shipping noise and background surface wind sound), s_q is the power level of the q^{th} ship source contributing to the acoustic field and $m_q(\theta)$ is the model predicted power at the location of source q, conditioned on environmental parameter vector θ. The dimension of the observation vector, respectively the model vector, is the number of sensors, in case multiplied by the number of frequencies. Note that a Bartlett type of objective function may not be used since it is a normalized quantity based on spatial/frequency correlation, and therefore insensitive to the absolute field intensity which is the goal here.

Assuming that the bathymetry is fixed, the two set of parameters to be included in optimization vector θ are water column and bottom properties. Changing water column sound speed by means of temperature profiles, mostly affects acoustic field structure and not so much attenuation. Acoustic field structure is represented by the bending of the propagation rays and therefore affects the signal time spread and depth dependence of the acoustic field. Instead changing bottom properties only affects shallow water propagation and has nearly no effect on signal attenuation in deep water, since rays seldom interact with the bottom in ocean depths over, say, 2000 m. In other words, in that case we see little, if any, chance of success in environmental parameter changes to significantly adjust model output to received levels.

5.2. Source Level adjustment

The actual source level of each passing-by ship is unknown so, in practice, characteristic values of each ship type (cargo, tanker, cruise, etc) drawn from the literature are normally used. Deviations between these typical values and actual emitted noise

intensity is unknown, but may potentially be quite large. The sum over the ship sources within acoustic reach may contribute to some degree of leveling of individual deviations if the number of sources is large and if ships are evenly distributed in the area. Otherwise, in some cases, a few close by passing ships may dominate the received field for short periods of time, introducing strong biases. Those biases and deviations may be frequency dependent.

A first attempt to directly estimate source levels of ships within acoustic reach of the receivers was proposed and tested with simulated data based on real AIS data, in [19]. The source model relies on several assumptions and the origin of possible errors is listed above. In this study, the first assumption made is stationarity, e.g. that ship radiated noise does not vary significantly in a given time window during which a least squares fit is attempted between model and observations by varying source ship levels. The goodness of the result depends on a Green's function matrix G that itself depends on the propagation model, environmental parameter vector θ and source positions given by AIS (named vector a in the paper). A simulated example is constructed based on 1 hour of true AIS data off the port of Lisboa (Portugal). In that case 17 different ships were identified as cruising by the observation location and inverted for the proposed technique. It is shown that even for the perturbed case, source level estimation accuracy is very high for close ships but steeply decreases with range / propagation conditions. This is normal because their respective weight in the received signal decreases accordingly. In the approach above the solution vector of ship source level is inherently assumed as deterministic.

An alternative would be to assume the source level as stochastic with a given probability density function (pdf) $p(P_{sl})$, as explored in the previous part. In this case the Bayesian estimator would be given, according to standard theory, by the conditional mean estimator (also called MAP - mean a posteriori),

$$\hat{P}_{sl} = \int_{\square} P_{sl}\, p(P_{sl} \vee o)\, d P_{sl} \ ,$$

where P_{sl} is the source level power variable and $p(P_{sl} \vee o)$ is the conditional pdf of P_{sl} when the observation vector o is known, also called the posterior pdf. In practice the problem remains that of estimating this posterior pdf that may be obtained through the well known Bayes relation

$$p(P_{sl} \vee o) = \frac{p(o \vee P_{sl})\, p(P_{sl})}{p(o)},$$

where:

1. $p(o \vee P_{sl})$ is the pdf of the observed data o when ship source level P_{sl} is known, and may be given by the model output for true source level vector;

2. $p(P_{sl})$ is the prior source level pdf before observation, which may be based on some previous historical observation. In order to take advantage of the Bayesian framework it would be desirable to assume a Gaussian prior, centered on historical source level values. This static may be built on existing source level models;

3. $p(o)$ is the prior pdf of the observations o, without dependence on the source level, this is a mere normalization factor.

Using the linear observation model proposed in [19] with the notation above, one may write the linear Bayesian observation data model as

$$x = Hs,$$

$$y = x + u,$$

where matrix H contains the Green's function transmission loss, s is the source level vector under estimation, assumed random and a priori Gaussian distributed $N(\mu_s, C_s)$ and u is the observation noise, assumed also zero mean white Gaussian distributed with variance σ_w^2 and uncorrelated with s. Without loss of generality C_s may be assumed diagonal or, in a first approximation, of the form $C_s = \sigma_s^2 I$. In that case estimator (8) may be expressed in closed form as:

$$\hat{s} = \mu_s + C_s H^T ¿$$

Several comments are in order:

1. The first comment is that the impact of the ill-conditioning of the Green's function matrix noted in [19] is substantially reduced here because the matrix to invert includes the noise cross-covariance;

2. The assumption of a Gaussian pdf for source level distribution makes more sense than a uniform prior, as normally used for poorly known a priori parameters. The mean of that distribution should be the historical values and constant variance σ_s^2 remains to be selected by trial and error;

3. In practice, since the true channel attenuation between each source and the receiver location is error prone, an estimate $\widehat{H}$ of H will be used in (13) so those model errors will be reflected in the final source level estimate, contributing to the data-model best fit;

In reality data model (12) only takes into account the shipping noise component, completely bypassing the surface wind sound background component. Although there might be local variations of wind speed induced surface sound, we will generally assume that ambient sound background component to be relatively stable over time so, we may model it as sound level $L_b(f)$ of a stochastic process power b with the usual Gaussian distribution $N(\mu_b, C_b)$. Therefore, a more realistic model, including the background component, would be

$$x = Hs,$$

$$y = x + b + u$$

Since $x = Hs$, b and u are all Gaussian distributed independent variables, their joint pdf is also Gaussian which implies that the posterior conditional distribution of $s \vee y$ is also Gaussian with mean

$$\hat{s} = E[s \vee y] = \mu_s + C_s H^T ¿$$

and covariance given by (adapted from theorem 10.3 in [20]),

$$C_{s \vee y} = C_s - C_s H^T ¿$$

Introducing suitable estimates for the a priori statistics of the source level s and the background b allows for computing the posterior estimators and its covariance as above. Also, the same framework may be used to derive the posterior of the predicted field estimate when the source level estimate is known, that is $p(y \vee \hat{s})$, and derive not only its conditional mean but also its variance at all spatial locations, therefore allowing to propagate the ship estimates near the observation locations to the whole area where shipping noise prediction is performed, as ships travel through the area.

5.3. Direct model transformation

The standard procedure follows to estimate sound maps in 1/3 octave frequency bands, represented by their center frequencies. To each center frequency in the band one may associate an SPL pdf drawn from the data observations and another one from the model predictions.

In theory, assuming a Gaussian distributed acoustic pressure, power SPL should be distributed according to a modified χ^2 with a number of degrees of freedom equal to the number of power bins averaged to obtain the SPL estimate. However, when the number of averaged bins is large the corresponding χ^2 distribution tends to approach the Gaussian distribution again, via the central limit theorem.

An ad hoc procedure to allow for data-model fitting much simpler and easier to implement than those proposed above, would be to perform a simple variable transformation from the model to the data distribution. The simplest example would be given by a linear transformation such as $Y = AX + B$ where B is a mean shift and A^2 represents a variance change coefficient. A different set of coefficients would be calculated for each frequency across the spectrum such that one would end up with a spectral calibration of the form $\{A(f_k), B(f_k); k = 1, \ldots, K\}$ for f_k being the 1/3 octave center frequency of the K frequency bands in, say, [40-1000] Hz. Note that this transformation is linear in the SPL domain but non-linear in the sound pressure power domain. In fact, if the level X is $X = 10 \log_{10} px$ and Y is $Y = 10 \log_{10} py$, then we will have $p_y = b p_x^a$, where $b = 10^{B/10}$ and $a = A$. This transformation ensures proper mean and variance shifts of the respective distribution but pdf shapes will not be preserved in the pressure level domain.

In practice this means that the SPL distributions over a given area would be (mean and variance) modified according to the differences between data and model found at the recording locations. The idea behind this is that mean and variance distribution modification would contain the model to data calibration necessary for each point in space. Although this view may be acceptable, its validity may be questioned for areas sparsely sampled in time and space, and its validation may be difficult if not impossible to ascertain. However, keeping these drawbacks in mind, the fact that this is the simplest route for field calibration this approach was tested in the Azores June 2018 data set as described in section 7-b.

6. Case study

6.1. Celtic sea

This section presents a case study performed in the Celtic Sea, using SHOM acoustic data recorded at station 04C and 05G (Figure 6.1.1). The modeling results are the JONAS preliminary noise maps computed for each day 2019. The modeled noise values were extracted at the closest positions and depth to the recorders and treated as time series vectors.

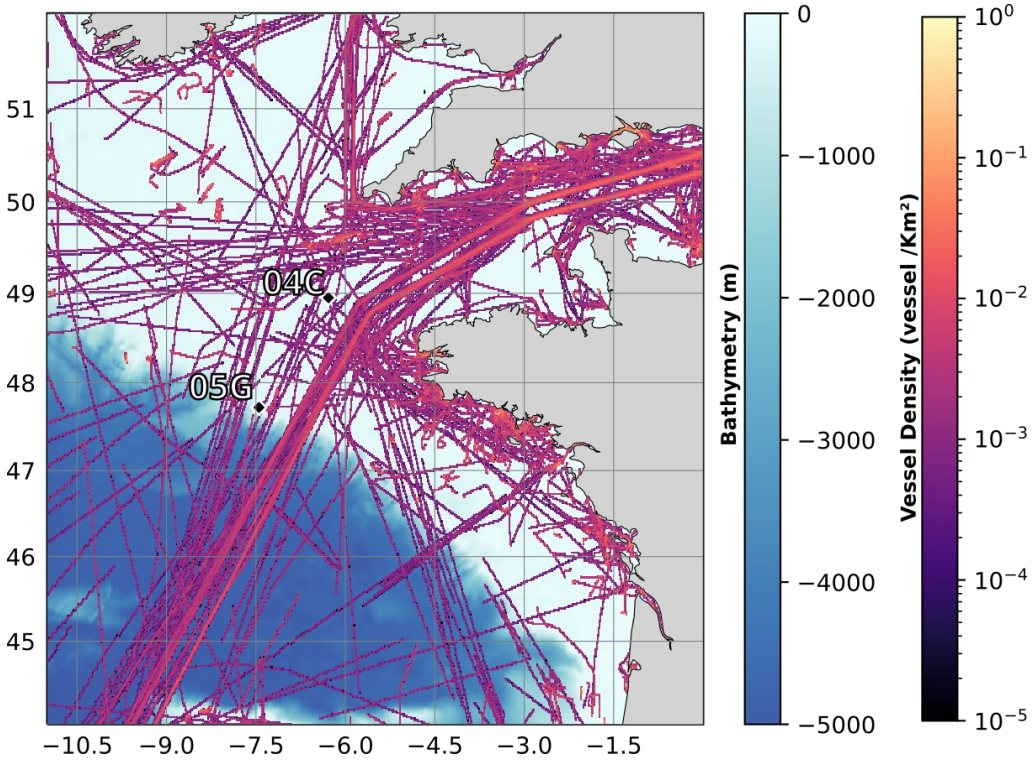

Figure 6.1.1: Bathymetry and vessel density map (total for the day 04-09-2019) with the recorder positions used in this case study (black diamonds).

6.1.1. Acoustic data

The acoustic data recorded at station 04C and 05G were processed at SHOM to produce a measured ambient noise level every 10 seconds for the OTO bands centered on 63 and 125 Hz. The 4 hydrophones deployed at each station have their location, depths and recording periods summarized in table T6.1.1.

Station	Position	n°Hydro	Depth (m)	T0	TF
04C	006°17,100'W 48°57,001'N	SMART 19	27	07/09/2019	22/10/2019
		SMART 1	37	07/09/2019	22/10/2019
		SMART 2	54	07/09/2019	10/10/2019
		SMART 3	83	07/09/2019	17/10/2019
05G	007°22,296' W 47°35,494'N	SMART 2	86	20/03/2020	23/05/2020
		SMART 3	155	21/01/2020	21/03/2020
		SMART 19	304	20/03/2020	18/05/2020

Table T6.1.1: Station 04C and 05G recorders, with their depth and recording periods.

The noise level density distributions were computed over the time series every 0.5 dB for both the measurements and the model. Additional processing was performed on the recorders of station 04C with the aim of reducing flow and self-noise. This processing was a selection of the time periods with the least currents observed in tide and current data (dark blue distributions in *Figure 6.1.2*). This step was only performed at station 04C in order to explore the gap between model and measurements and was found to be very relevant.

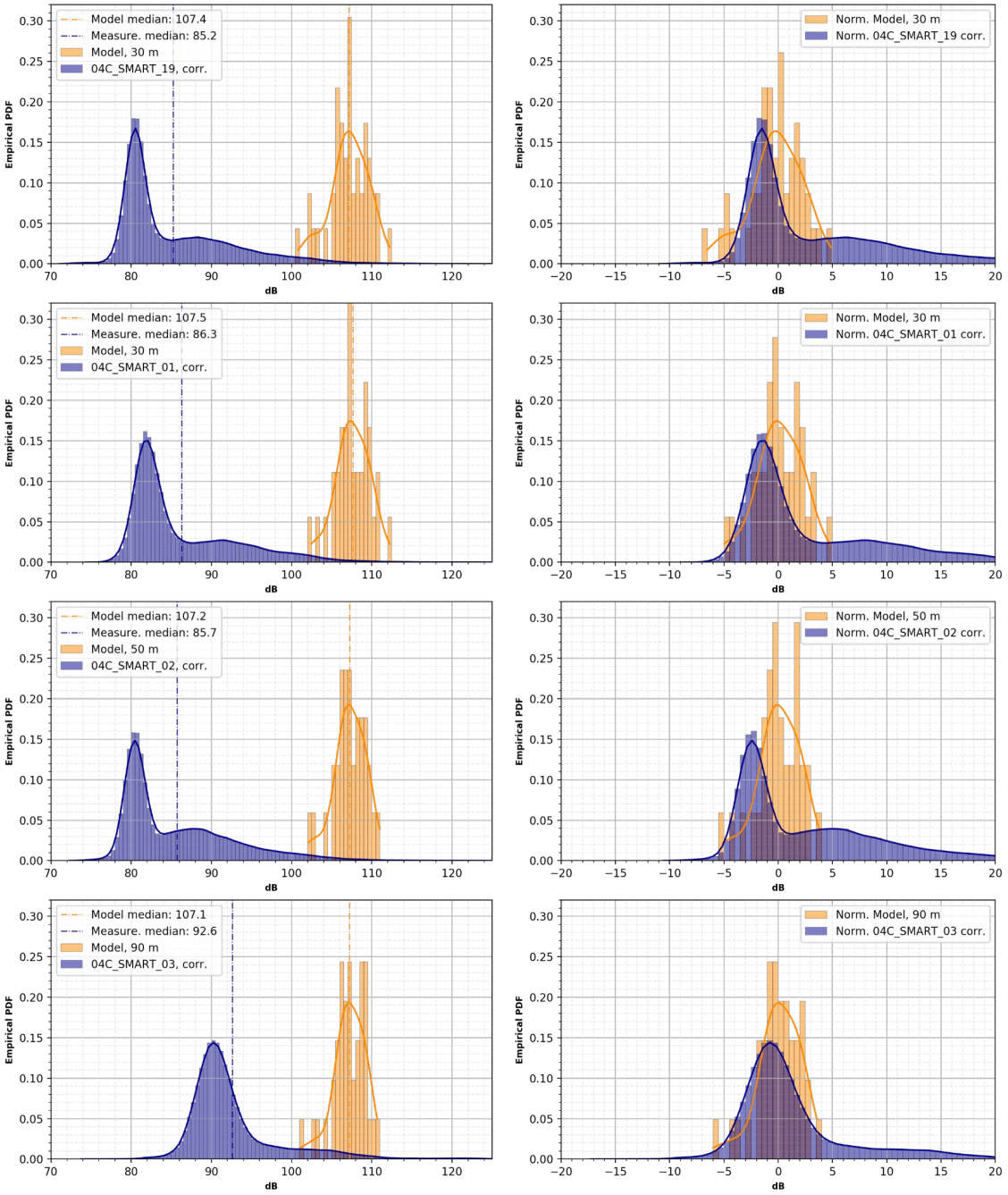

Figure 6.1.2: ***Left****: Noise level distributions measured and modeled at station 04C.* ***Right****: Noise level distributions with each value normalized to the median level observed in the left plot. Modeled distributions are in orange; Dark blue is the measurement distribution with a time selection with the least flow noises. The heavy tail observed in the measurements distribution mainly results from self-noise that is problematic on this recorder, as well as some rare and close passages of vessels.*

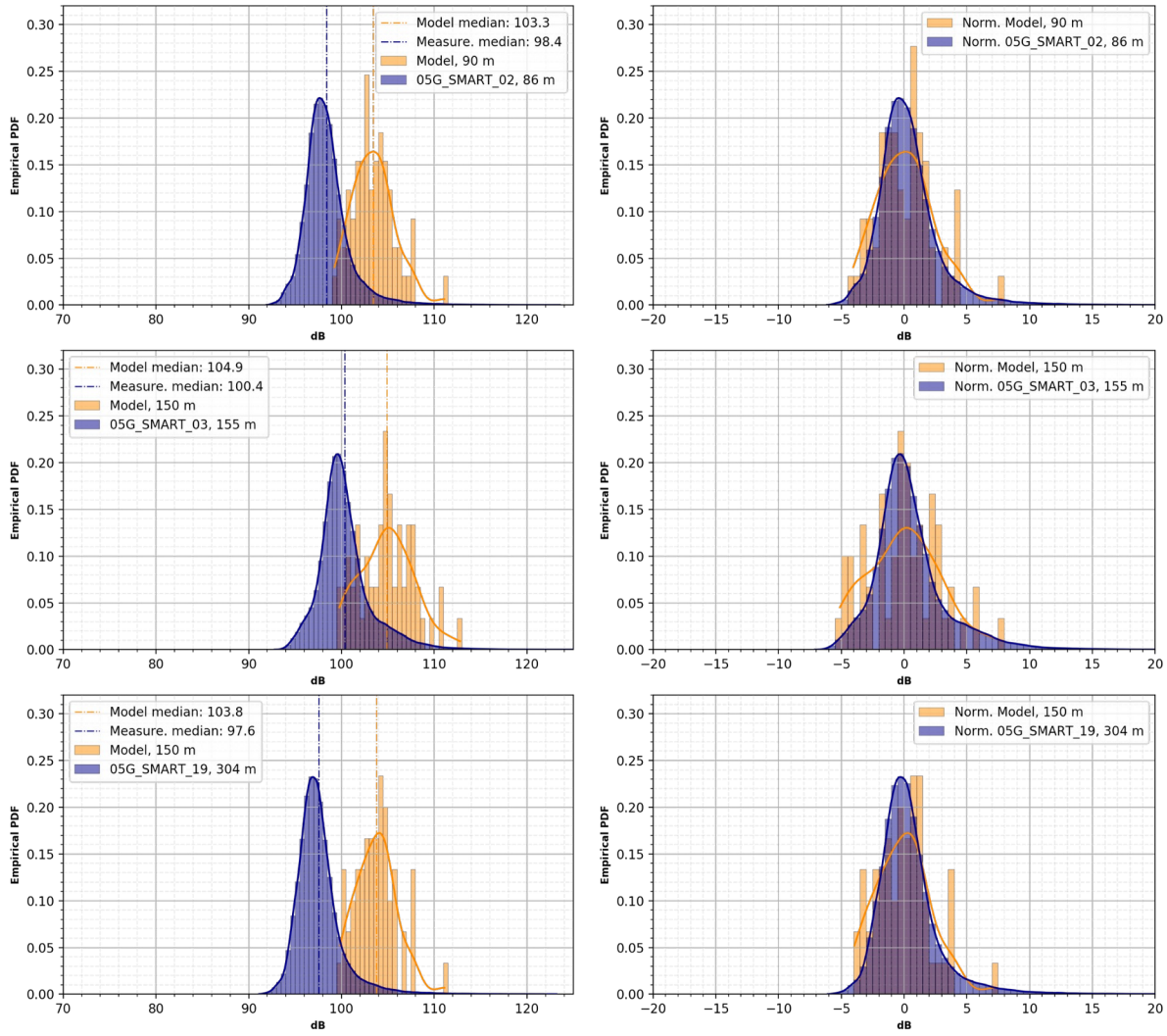

Figure 6.1.3: ***Left****: Noise level distributions measured and modeled at station 04C.* ***Right****: Noise level distributions with each value normalized to the median level observed in the left plot. Modeled distributions are in orange; Dark blue is the measurement distribution with a time selection with the least flow noises.*

6.1.2. Comparison results

Comparison was performed following the methodology described in this document by computing the statistical moments, the Minkowski and Sørensen similarity between the measured and modeled noise level distributions (empirical PDF). Results are shown in the next tables (A-T2) and figures (6.1.2 to 6.1.3).

	Model			Processed Measurements		
station	**Mean**	**Median**	**SD**	**Mean**	**Median**	**SD**
05G_SMART_03	104.88	104.90	2.89	100.36	99.91	2.88
05G_SMART_19	103.75	103.80	2.21	97.56	97.20	2.47
05G_SMART_02	103.42	103.30	2.27	98.40	98.07	2.44
04C_SMART_19	107.16	107.37	2.41	85.24	82.04	6.85
04C_SMART_01	107.61	107.46	2.10	86.31	83.35	6.76
04C_SMART_02	107.26	107.20	1.94	85.73	82.88	6.90
04C_SMART_03	107.17	107.12	1.98	92.61	91.01	5.80

Table T6.1.2: Resulting analysis of the statistical moments for all the hydrophones at the station 05G and 04C. 04C measurements analysis was performed on the flow-noise processed values.

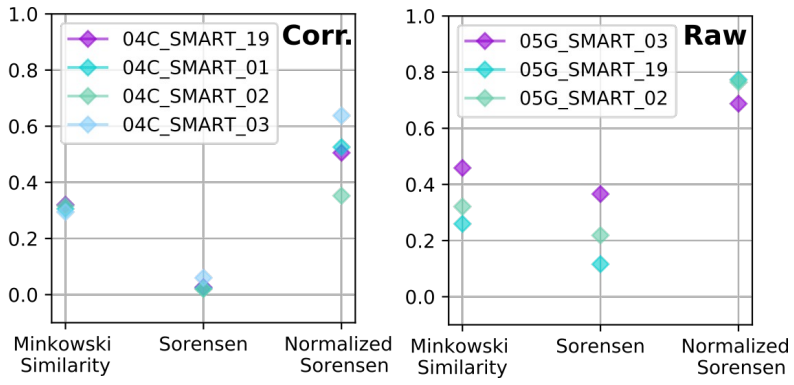

Figure 6.1.4: Minkowski and Sørensen similarity computed between the modeled and measured noise level distributions (empirical PDF) for all the hydrophones at both stations 04C and 05G. 04C measurements analysis was performed on the raw data and the flow-noise corrected values.

The results obtained from this analysis show a large difference between the two stations, with the 05G model being closer to the measurements than the ones at 04C. Still, the modeled noise level distributions are higher than the measured ones at both stations.

Results from the statistical moments measured and modeled at the station 04C show a large discrepancy between hydrophones. A minimal median or mean difference is found at the hydrophone 04C_SMART_03, which corresponds to the deepest hydrophone of the station. Here the

use of the similarity methodology allows to quantify this difference, and it is showing a very low Sørensen similarity. This means that the two distributions are largely different.

The three remaining hydrophones show similar median and mean differences between measurements and model (21 to 25 dB offset). This difference is less pronounced with the raw measurements than with the flow noise processed data shown here. The normalized Sørensen similarity computed between the flow noise processed measurements and the model, show a rather average fit between the distribution's shapes and over the 4 hydrophones. The Minkowski method has returned values that are close to 0.5. The small variations around this central value are in agreement with the results from the Sørensen method.

For the station 05G the model and measurements are distant by approximately 5 dB in mean and median values. The standard deviations of both distributions are very close (difference of variances is approx. 1 dB). This is also observed in the high values of normalized Sørensen similarities, meaning that the shapes of the distribution are close.

6.1.3. Confidence assessment

These results can be summarized in terms of uncertainty with the Table T6.1.3 assessed using the mean level error and the shape of the distribution for the temporal dynamic. Here, the local differences between stations are of 5 dB in mean at 05G station, and more than 20 dB at 04C. Moreover, the fit between the distribution shapes, means that temporal dynamics of the noise levels are matched in both cases. These results could mean that the model is affected by a systematic error locally. At station 04C, the calibration process could be oriented toward a work on the seabed parameters.

The confidence radius was computed following the methodology exposed above by using the TL modeled at 63 Hz and presented in figure 6.1.5. The table T6.1.3 summarizes the information of uncertainty estimated qualitatively from the distributions, for both stations and confidence radius on this uncertainty estimation.

	04C	**05G**
Error mean levels	High	Average
Error Dynamic	Low	Low
Empirical confidence radius (km)	77.13	93.83

Table T6.1.3: Qualitative confidence assessment results for the two stations 04C and 05G evaluated in this case study.

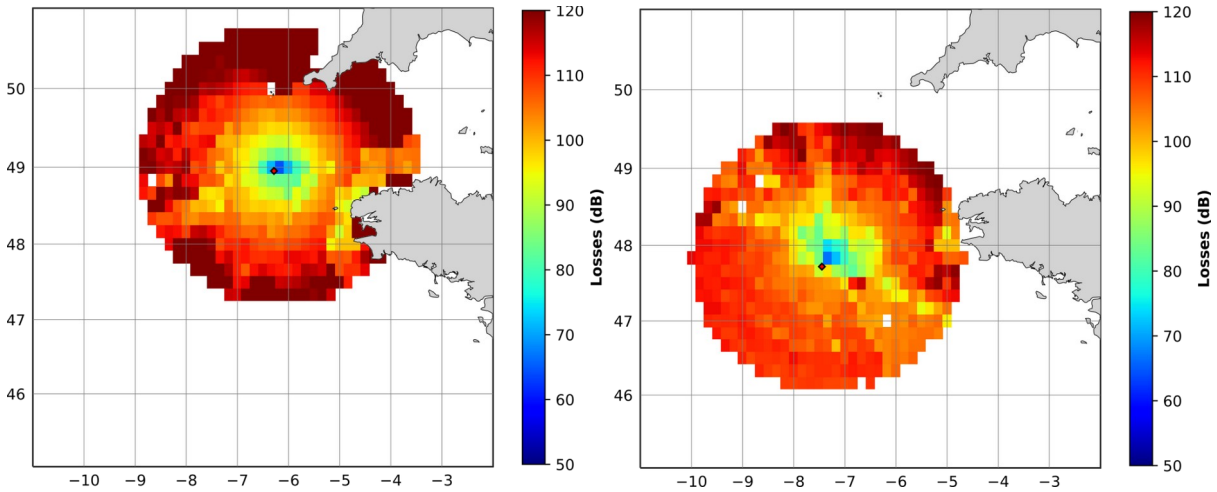

Figure 6.1.5: Representation of the transmission losses associated with the position 04C (left) and 05G (right). Computed at 63 Hz using RAMS and SHOM datasets.

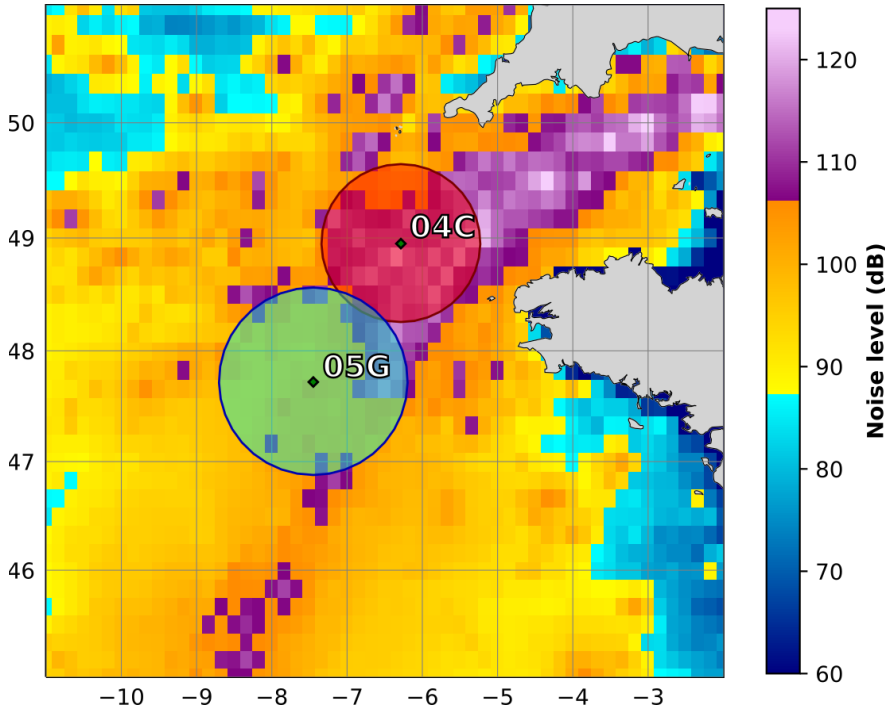

Figure 6.1.6: Noise map of the day 17-03-2019 for the One Third Octave band centered on 63 H Colored circles represent the confidence radius defined in the table T6.1.3 at both stations 04C and 05G. The color is based on the error on the mean levels from this table.

Figure 6.1.6 represents the radius of confidence around both receivers and the qualitative error estimation as colors. The recorder 04C is affected by self-noise and strong current induced noises, which is also limiting the confidence in the comparison results. This confidence in the acoustic data processing was not incorporated in this study, but it could eventually be added in table T6.1.3 while the color could be adjusted to summarize all the information.

6.2. Case study Azores

This section describes the application of the field calibration methodology described in (section) to the data set provided by the IMAR-Okeanos group in the Faial - Pico Islands study area in the Azores. Figure 6.2.1 shows the bathymetry of Azores central group of islands as given by GEBCO [21]. The black box signals the area where three IMAR-Okeanos acoustic recorders are located.

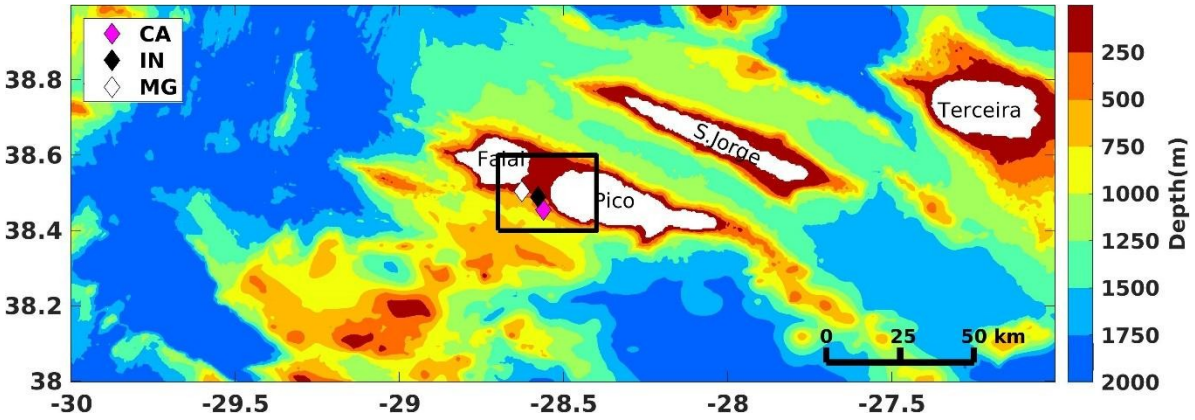

Figure 6.2.1: Central Azores archipelago bathymetry map covering the islands of Faial, Pico, S.Jorge and Terceira with box signaling IMAR-Okeanos acoustic recorders position.

6.2.1. Acoustic data

The box with the acoustic recorders is shown in great detail in Figure 6.2.2. The location of the acoustic recorders is shown as the colored diamonds: CA on the Pico side at 484m depth, IN at the channel border and MG on the Faial slope both at 200m depth.

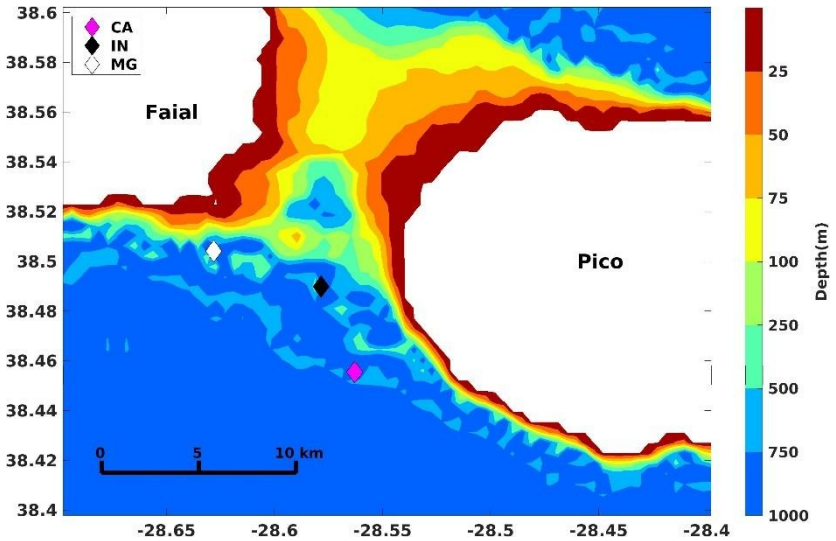

Figure 6.2.2: Faial - Pico bathymetry with CA, IN and MG recorder positions.

The data was recorded with three Ecological Acoustic Recorders (EAR) produced and commercialized by Marc Lammers [22]. These are duty cycle programmable long endurance deep

water recorders with an assumed flat sensitivity over the band 20 - 1000 Hz, operated at a sample rate of 2000 Hz, 16-bit resolution and a 47.5 dB total chain gain.

The data was read and processed with the PAMGuide package[1] The SPL was calculated at the 16 one-third octave band center frequencies in the band 20-1000 Hz, as the sum of the power spectra estimates over each one-third octave band. The power spectra estimates were obtained for 1 s window length (*i.e.* a frequency spacing of 1 Hz) and averaged over 10 min. The EARs were set to record from 14:00 to 20:00 UTC each day. Internal clock drift exists but is unknown, so data validation through individual target tracking is only approximative.

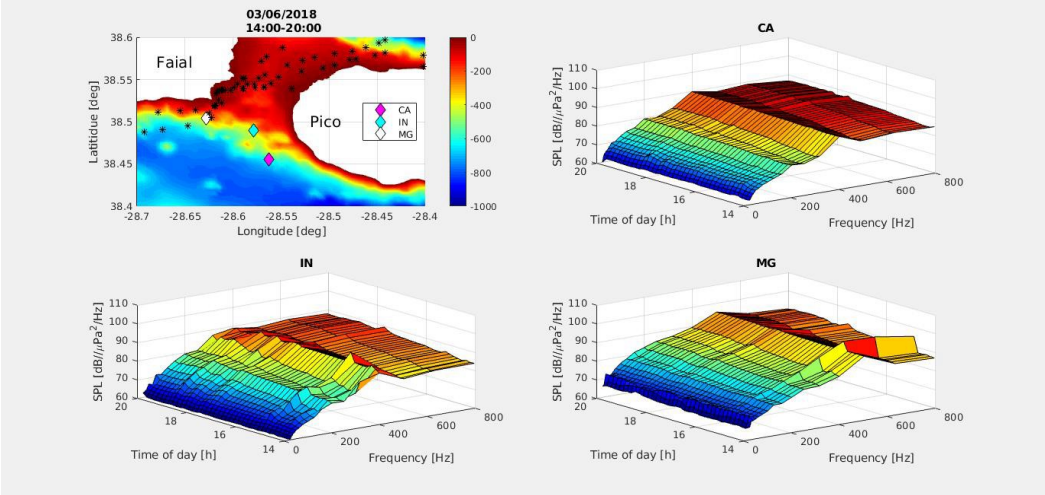

Figure 6.2.3: Data collected on June 3, 2018 from 14h to 20h UTC: bathymetry, recorder position and AIS cumulative ship distribution (top left); measured SPL over time of the day and frequency in the band 20 - 1000 Hz for CA (top right), IN (bottom left) and MG (bottom right).

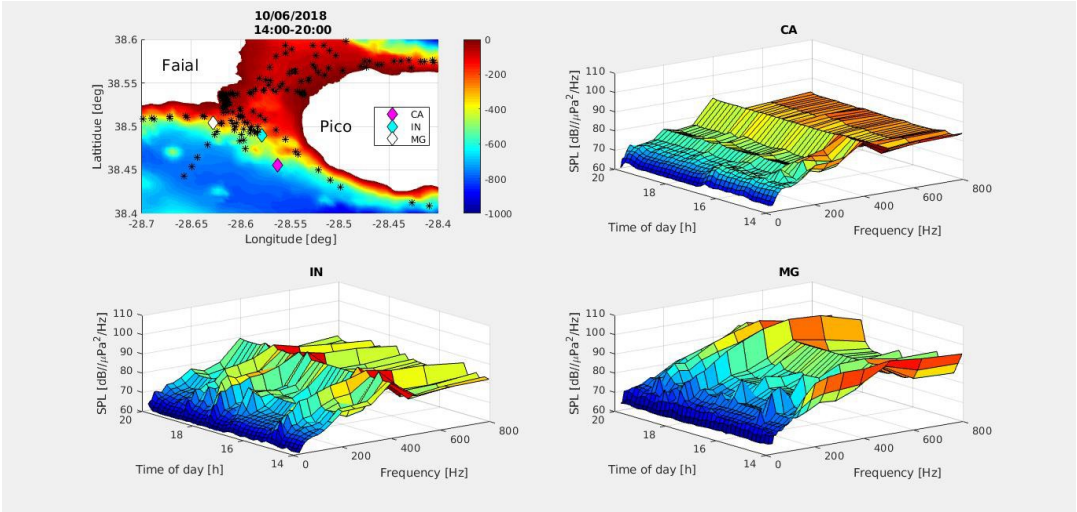

Figure 6.2.4: Data collected on June 10, 2018 from 14h to 20h UTC: bathymetry, recorder position and AIS cumulative ship distribution (top left); measured SPL over time of the day and frequency in the band 20 - 1000 Hz for CA (top right), IN (bottom left) and MG (bottom right).

1 https://doi.org/10.1111/2041-210X.12330reference PAMGuide paper, including Matlab and R codes supplementary information.

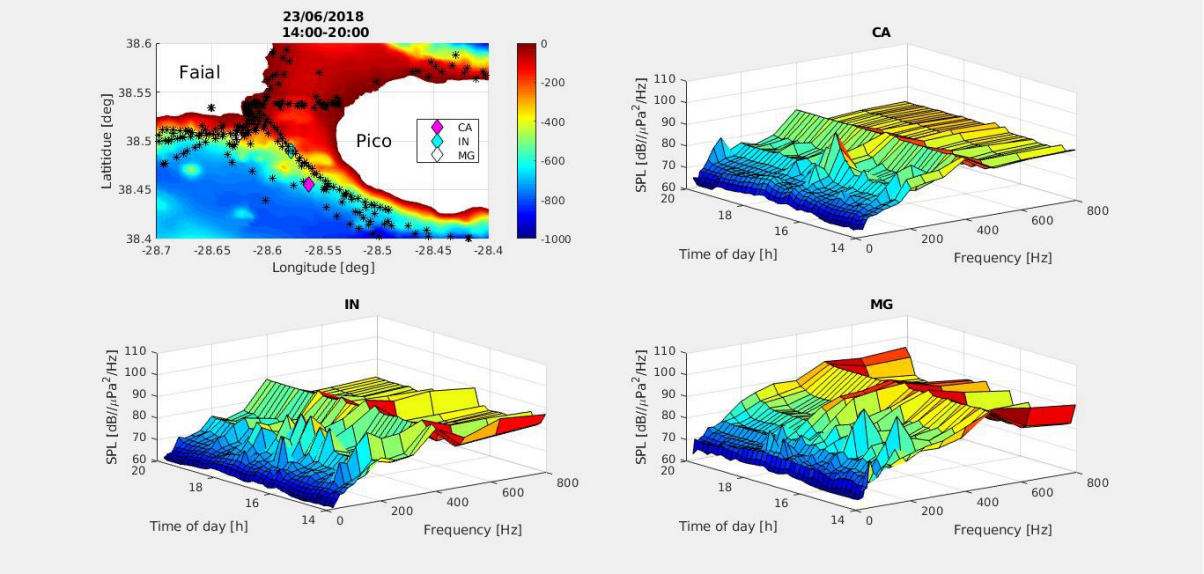

Figure 6.2.5: Data collected on June 23, 2018 from 14h to 20h UTC: bathymetry, recorder position and AIS cumulative ship distribution (top left); measured SPL over time of the day and frequency in the band 20 - 1000 Hz for CA (top right), IN (bottom left) and MG (bottom right).

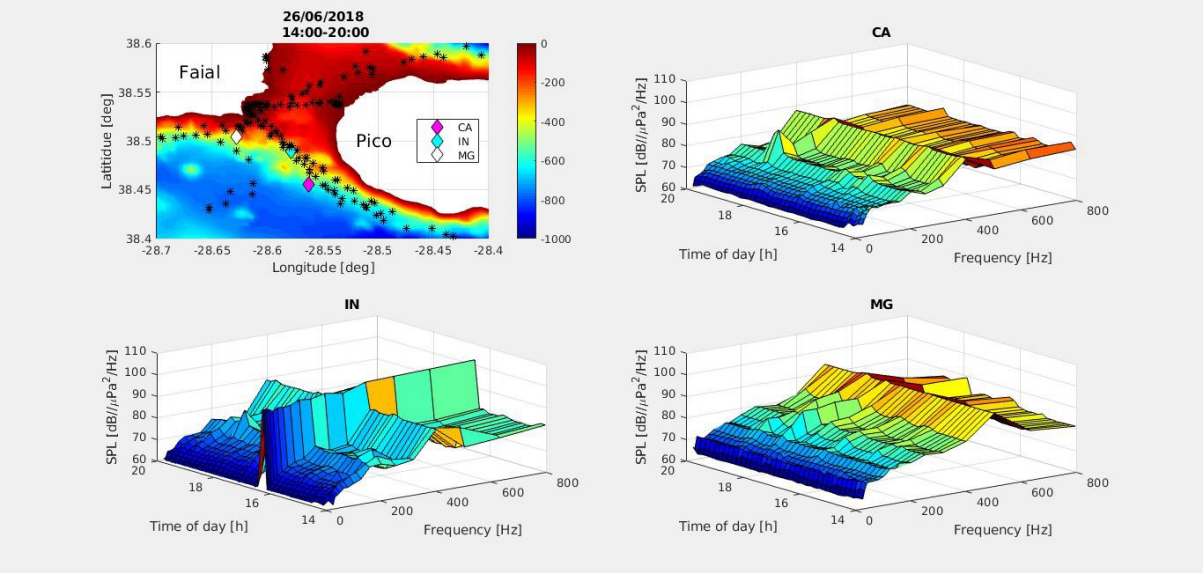

Figure 6.2.6: Data collected on June 26, 2018 from 14h to 20h UTC: bathymetry, recorder position and AIS cumulative ship distribution (top left); measured SPL over time of the day and frequency in the band 20 - 1000 Hz for CA (top right), IN (bottom left) and MG (bottom right).

As illustrative examples, figures 6.2.3 – 6.2.6 show the recorded data for days 3, 10, 23 and 26 of June 2018. Each figure shows the bathymetry and cumulative AIS ship location distribution between 14:00 - 20:00 for the area at hand (top left) and then clockwise the measured SPL over time of the day and frequency at the CA, MG and IN sites. A short movie with the received spectra for all days of June 2018 is available as supplementary material to this report.

It is relatively standard to analyze the statistical behavior of an ocean sound data set through spectral power histograms. These are shown in Figure 6.2.7, for the received data at the three locations CA, IN and MG in plots (a) to (c), respectively. These figures were obtained for 1 s time windows, therefore with a spectral resolution of 1 Hz, with 50% time overlap but no averaging. Therefore, these are not power spectral estimates but "sample power spectra". The color scale denotes empirical probability so, SPL sample count on each interval over total number of samples, for each frequency.

(a) (b) (c)

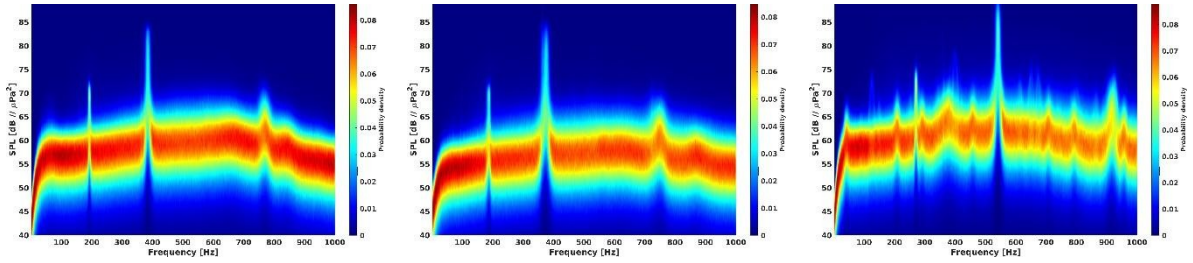

Figure 6.2.7: Faial-Pico data set spectral power distribution with 1 second time slots between 14:00 and 20:00 UTC in June 2018 for CA (a), IN (b) and MG (c).

Some preliminary comments are in order:

1 The output spectra is strongly attenuated in the low frequency band below, say 60 Hz. Whether that is an imposed high-pass filter in the acquisition chain to avoid static pressure oscillations or a loss of sensitivity of the hydrophone for that frequency band, is not known at this stage.

2 Abnormally resistant intensity peaks can be seen at some individual frequencies; those are persistent along time and vary from one recorder to the other. In fact, the recorders at CA and IN are quite similar with a strong peak at 380 Hz and two smaller at 200 and 800 Hz, while MG has several clear peaks with a very strong one at 530 Hz. Clearly, those peaks are hardware related and the generated self-noise greatly limits the system capabilities in those frequency bands;

3 Taking into account these observations, the filters of table 1 were applied to the data prior to their usage for model calibration.

	Cut bands
CA	188-197 and 374-393 Hz
IN	184-191 and 357-387 Hz
MG	267-274 and 528-553 Hz

Table 6.2.1: Band cut frequency filters applied to the observed recorder data

6.2.2. Shipping noise modeling

Shipping noise modeling was performed by Marsensing using a methodology described in [23] and the following data sets: AIS data shared by AIShub[2], the source level from McKenna [24], and the Kraken propagation model fed with the GEBCO bathymetry [21], the water column predictions by CMEMS[3] and a uniform bottom description, as briefly shown in appendices 6.1 and 6.2. The results of the shipping noise modeling are discussed in detail in [25], [26]. The time and space grids were set to 10 minute and 500m×500m, respectively. In a first stage the field was projected onto the locations of the receivers and a time series for each frequency was obtained, every 10 min for the whole month at each location CA, IN and MG. Figure 6 shows the predicted shipping noise SPL only for each time of day and day of month for the three locations CA (a), IN (b) and MG (c).

(a)

2 https://www.aishub.net/ https://www.aishub.net/

3 https://marine.copernicus.eu/https://marine.copernicus.eu/

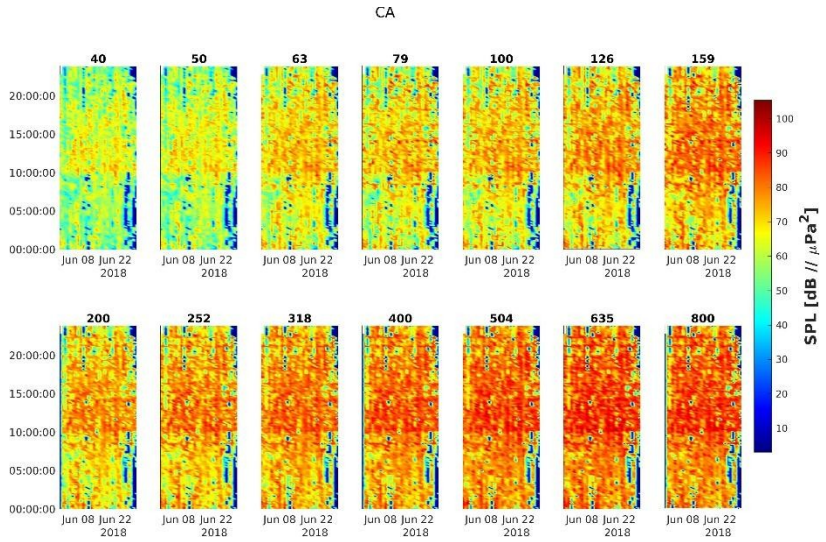
CA
40
50
63
79
100
126
159
200
252
318
400
504
635
800
20:00:00
15:00:00
10:00:00
05:00:00
00:00:00
Jun 08 Jun 22
2018
SPL [dB // µPa²]
100
90
80
70
60
50
40
30
20
10

(b)

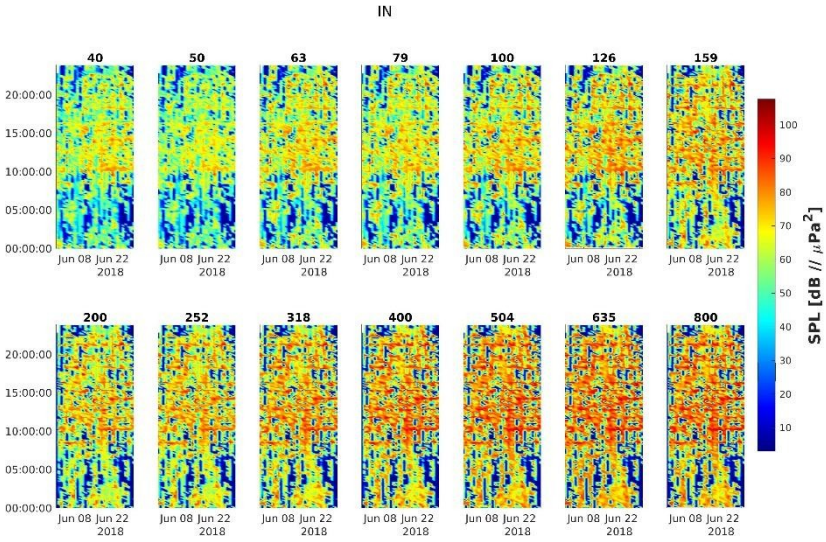
IN
40
50
63
79
100
126
159
200
252
318
400
504
635
800
20:00:00
15:00:00
10:00:00
05:00:00
00:00:00
Jun 08 Jun 22
2018
SPL [dB // µPa²]
100
90
80
70
60
50
40
30
20
10

(c)

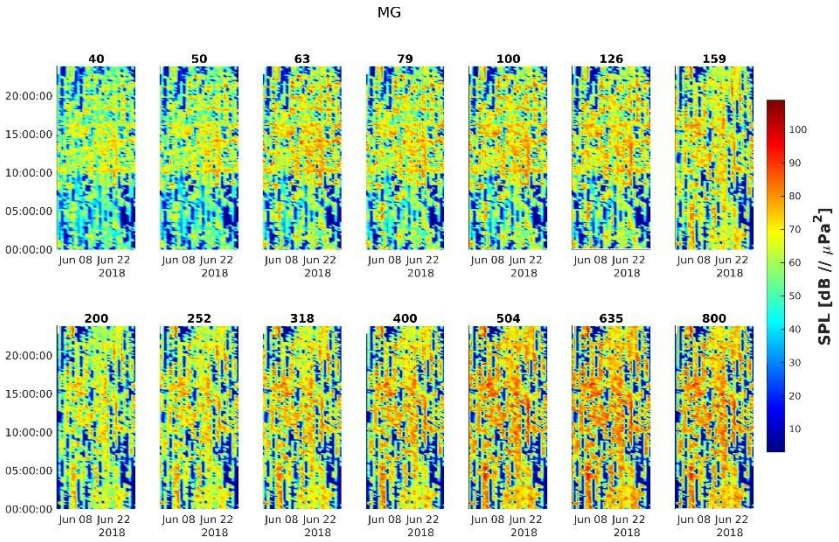

Figure 6.2.8: Model shipping noise for each frequency band as a function of time of the day and day of the month for sites CA (a), IN (b) and MG(c).

Clearly there is an SPL increase at some hour between 09:00 and 10:00, almost for all days of the month, in all channels and frequency bands. That increase is stronger at CA sites than at IN and MG. There are a number of days and times with nearly no noise (possibly no ships). These noise "empty" moments are more frequent during the night and at the IN and MG sites.

6.2.3. Wind noise modeling

The wind noise forecast database from the European Center for Medium-Range Weather Forecast (ECMWF)[4] for the whole month of June 2018 was used. The coverage is from [-32˚,-10.25˚] longitude West and [30˚,39.75˚] latitude North, as shown in appendix 6.3. The corresponding mean broadband wind sound level is shown in Figure 6.2.10[5] Clearly the month of June mean wind generated sound, at least for this broadband component, is nearly constant at around 89 dB re μPa^2.

4 https://www.ecmwf.int/ https://www.ecmwf.int/

5 for islands names please refer to figure 2, these will not be marked in the following plots to avoid image cluttering and for a lack of space.

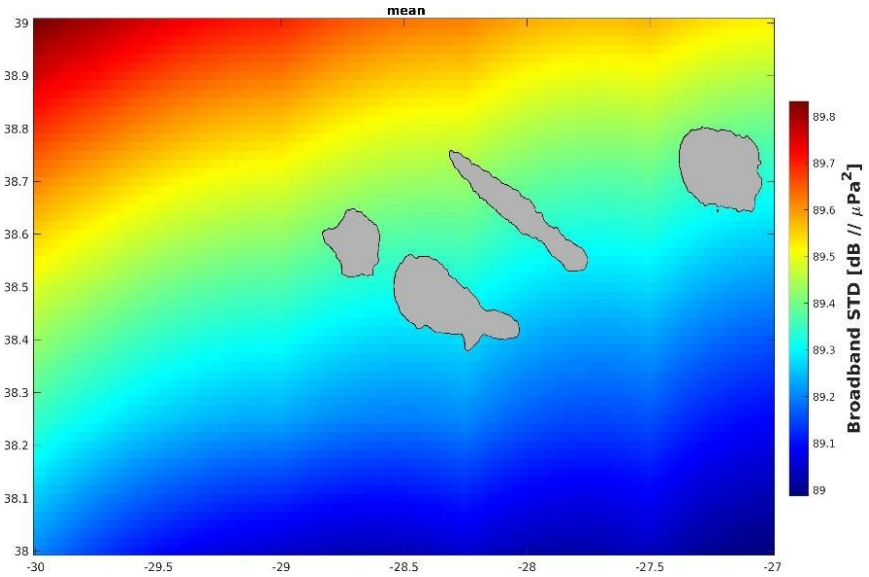

Figure 6.2.9: Azores wide area over the whole month mean broadband SPL generated with the wind Kewley et al. wind model using the ECMWF data.

6.2.4. Shipping noise and surface wind generated sound model

Putting together surface wind sound and shipping noise modeled with the tools described above, for the three recording sites CA, IN and MG one gets the surfaces shown in Fig. 6.2.10(a), (b) and (c), respectively.

(a)

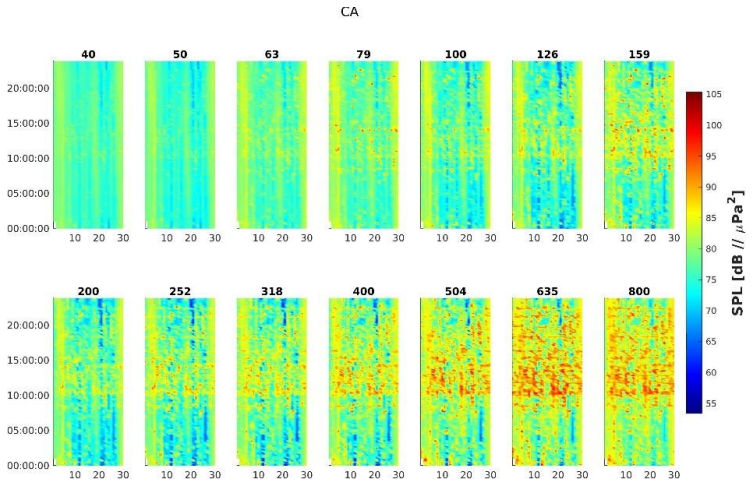
CA
40
50
63
79
100
126
159
200
252
318
400
504
635
800
20:00:00
15:00:00
10:00:00
05:00:00
00:00:00
10 20 30
SPL [dB // µPa²]
105
100
95
90
85
80
75
70
65
60
55

(b)

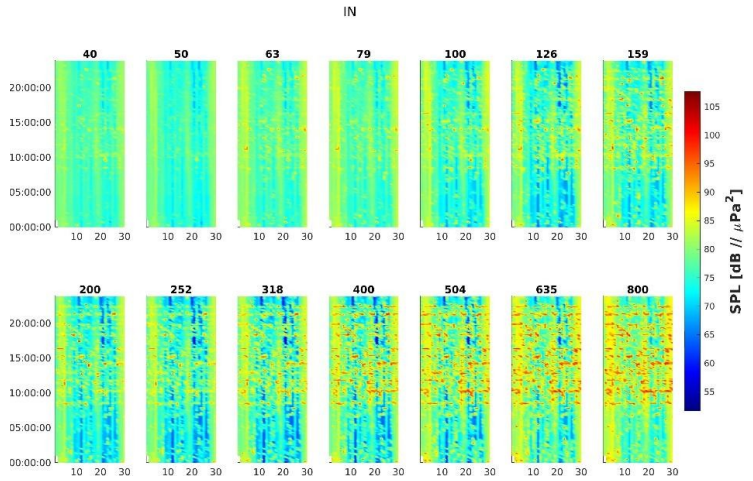
IN
40
50
63
79
100
126
159
200
252
318
400
504
635
800
20:00:00
15:00:00
10:00:00
05:00:00
00:00:00
10 20 30
SPL [dB // µPa²]
105
100
95
90
85
80
75
70
65
60
55

(c)

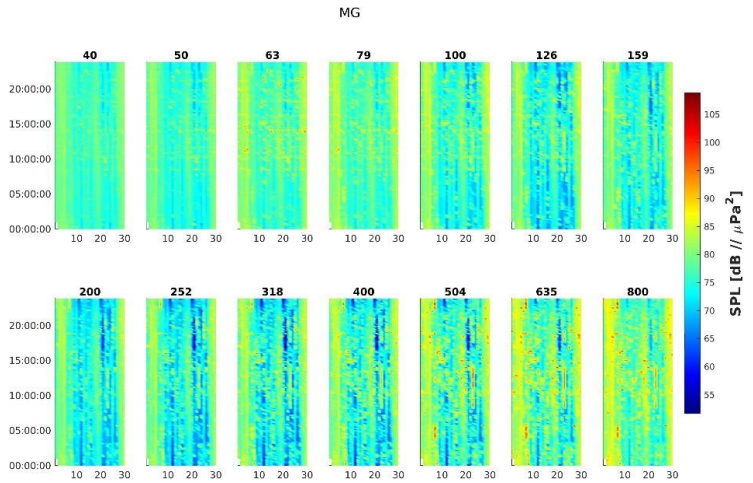
MG
40
50
63
79
100
126
159
200
252
318
400
504
635
800
20:00:00
15:00:00
10:00:00
05:00:00
00:00:00
10 20 30
SPL [dB // µPa²]
105
100
95
90
85
80
75
70
65
60
55

Figure 6.2.10: Model shipping and wind noise for each frequency band as a function of time of the day and day of the month for sites CA (a), IN (b) and MG (c).

It is clear that the noise "holes" are now filled with the background surface wind generated sound that shows different levels according to each frequency band. Note also that the color bar with SPL has now a minimum level of 52 dB. The background level varies along the day of the month and according with frequency but it is the same for recorders CA and IN that are in the same wind cell, and slightly different for MG, lying in the contiguous wind cell.

6.2.5. Data-model - comparison

Data and model SPL may be compared for the three recorder locations by means of the SPL empirical distributions which are proxies of the probability density function (pdf) of energy distribution. These are shown for each 1/3 octave frequency bands and broadband in Fig.6.2.11(a), (b) and (c), for CA, IN and MG, respectively: observed data (red), modeled data (blue) and field calibrated data (green).

(a)

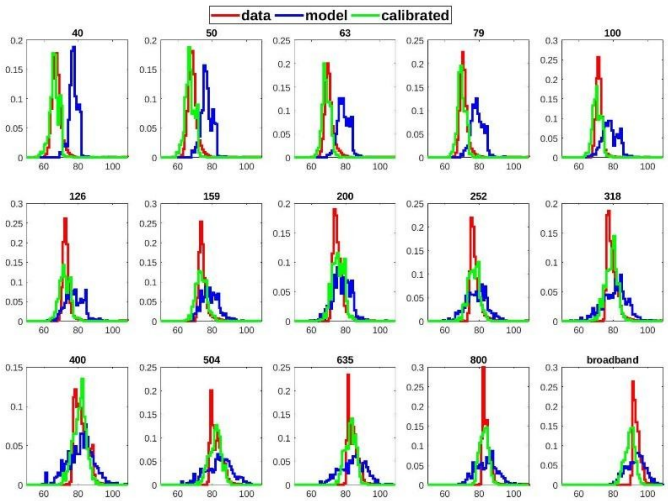

(b)

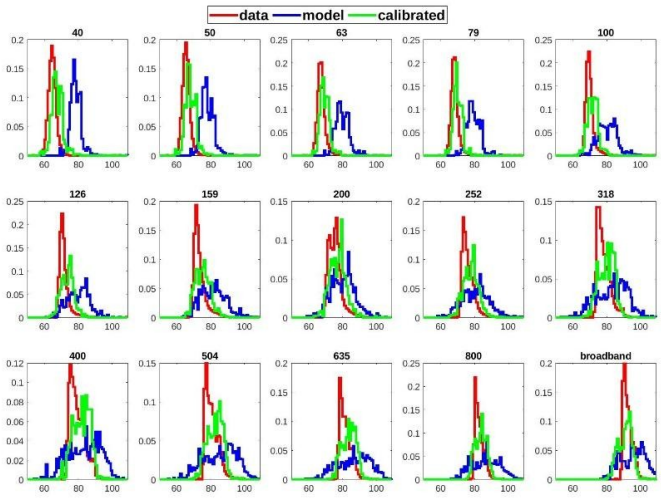

(c)

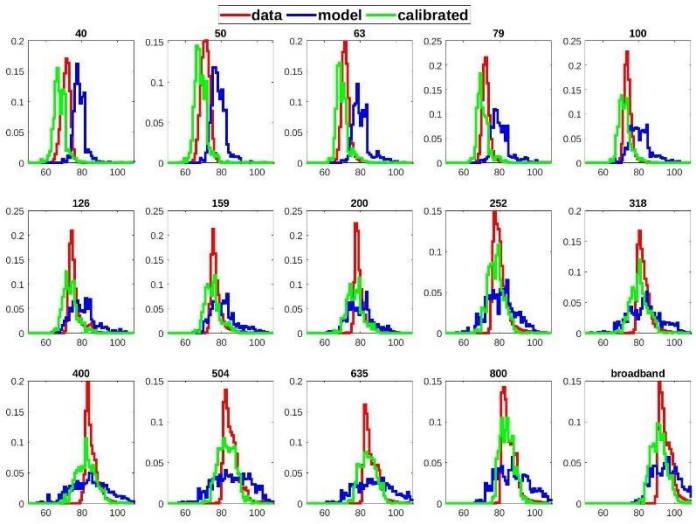

Figure 6.2.11: Data - model comparison of empirical probability of SPL distribution for 1/3 octave bands in 40-1000 Hz and broadband for June 2018 from 14:00 to 20:00 UTC for CA (a) IN (b) and MG (c): data (red), model (blue) and field calibrated (green).

The first remark is that the model noise distribution (in blue) tends to overestimate the data (in red) in the low frequency bands, say those below 126 Hz. In the upper bands the model and the data distribution tend to be centered with, however, a much smaller variance for the data than for the model. Even the 200 and 400Hz bands in the CA recorder and the 200 and 500Hz for MG are

now relatively centered. This behavior is due to the filtering imposed on the self-noise corrupted bands as seen on Fig. 6.2.12. The distributions after calibration (in green) were obtained by the linear transformation in the SPL domain as explained above. Since the ensemble of observations of CA, IN and MG were put together in a single distribution from which the transformation coefficients were calculated, their projection for each recorder location does not exactly fit the data distribution but clearly tends to it, as it can be observed in the figures. The objective of this ensemble of data is to provide a more spatial robust calibration than if a single recorder was used. The broadband field (shown in the bottom right plot of each figure) was calculated as the power sum of the 1/3 octave frequency bands over the whole considered band.

6.2.6. Wide area shipping and wind modeling

The next step is to extend the modeling to the wide area of the several islands and the surrounding stretch of ocean of the Azores central group archipelago, for the whole month of June 2018. That is shown in Fig. 9 for the field received at 10 m depth, as the time mean SPL for the usual 1/3 frequency bands between 40 and 1000 Hz.

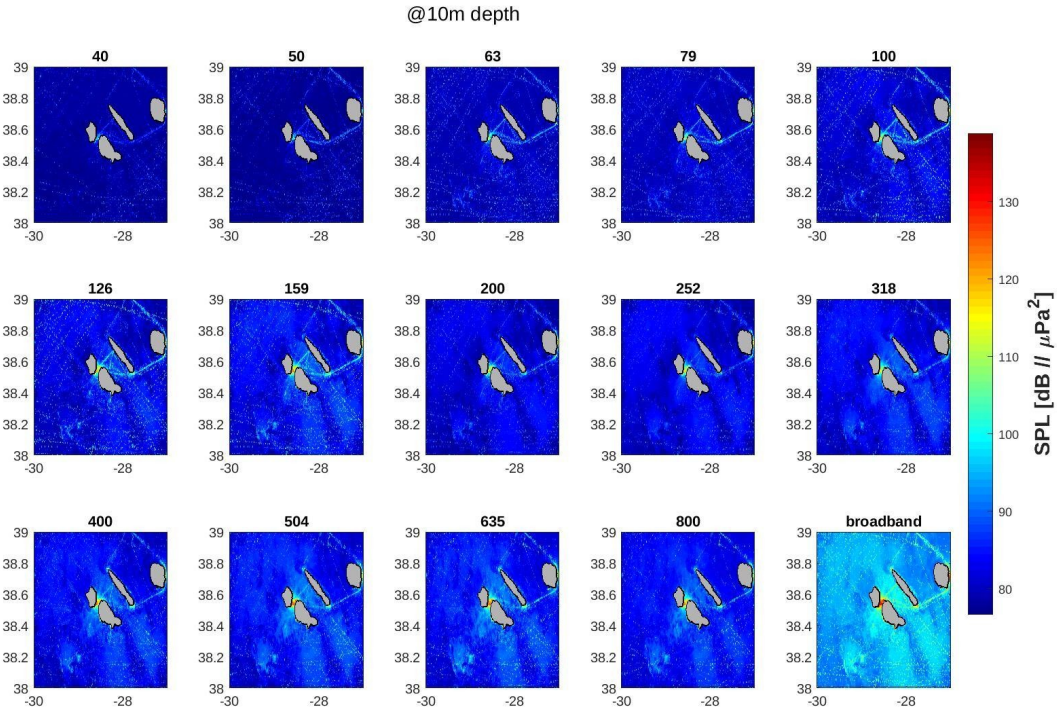

Figure 6.2.12: Modeled field: time mean at 10 m depth for the 1/3 octave frequency bands in 40-1000 Hz and broadband, for June 2018 at 10 min average with a 500 m spatial resolution.

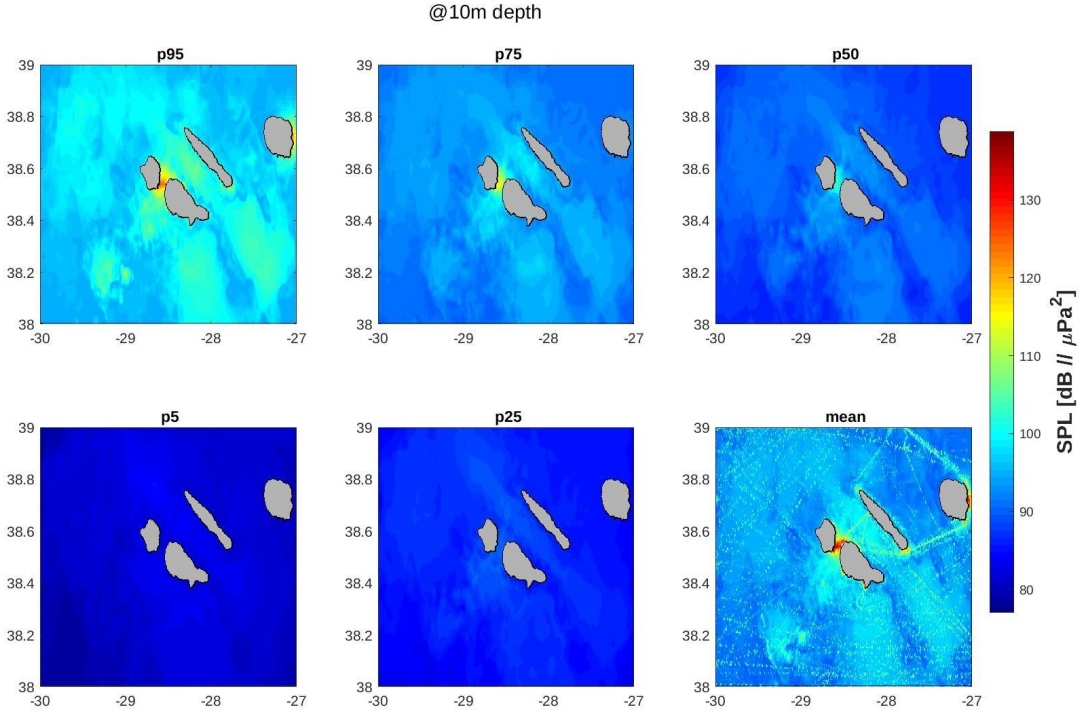

Figure 6.2.13: Broadband modeled field: 5, 25, 50, 75 and 95% percentiles and time mean at 10 m depth in 40-1000 Hz, for June 2018, 10 min average with a 500 m spatial resolution.

The field distribution is clearly modulated through frequency with shipping routes between islands and in other areas to the southeast being enhanced for the upper frequency band. The statistics for the broadband case is shown in Fig.6.2.13 for the 95, 75, 50, 25 and 5 percentiles and the mean, for the same modeled data. Note that the broadband field is obtained, for each time sample, as the power sum over the whole frequency band of the 1/3 center frequencies. The percentiles are extracted from the empirical cumulative density function obtained from histogram of these time samples over the whole month and for each lat-lon location.

6.2.7. Field calibrated of wide area shipping and wind model data

As mentioned above the adopted strategy is to apply the simple calibration method based on a linear transformation of the model distributions throughout space for each frequency band. The coefficients of the transformation were deduced from the comparison between the modeled data and the data gathered at the three, CA, IN and MG sites for each afternoon between 14:00-20:00 UTC during the whole month of June 2018. The data of each recorder was filtered according to the frequency bands shown in table 1. These coefficients introduce a SPL mean shift or variance spread modification, depending on the frequency. Figure 11 shows the whole month time means on each frequency band and then for the broadband case (bottom right).

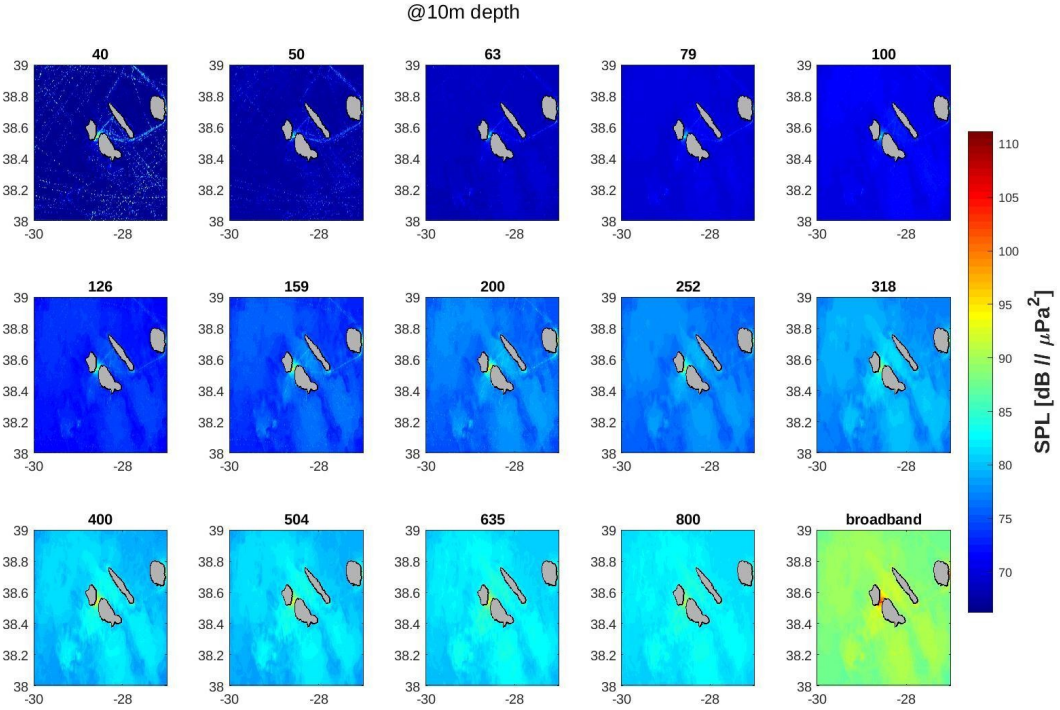

Figure 6.2.14: Field calibrated modeled field: time mean at 10 m depth for the 1/3 octave frequency bands in 40-1000 Hz and broadband mean, June 2018, 10 min average.

The statistics for the broadband case are shown in Fig. 12 for the 95, 75, 50, 25, 5% percentiles and the mean, for the same modeled data.

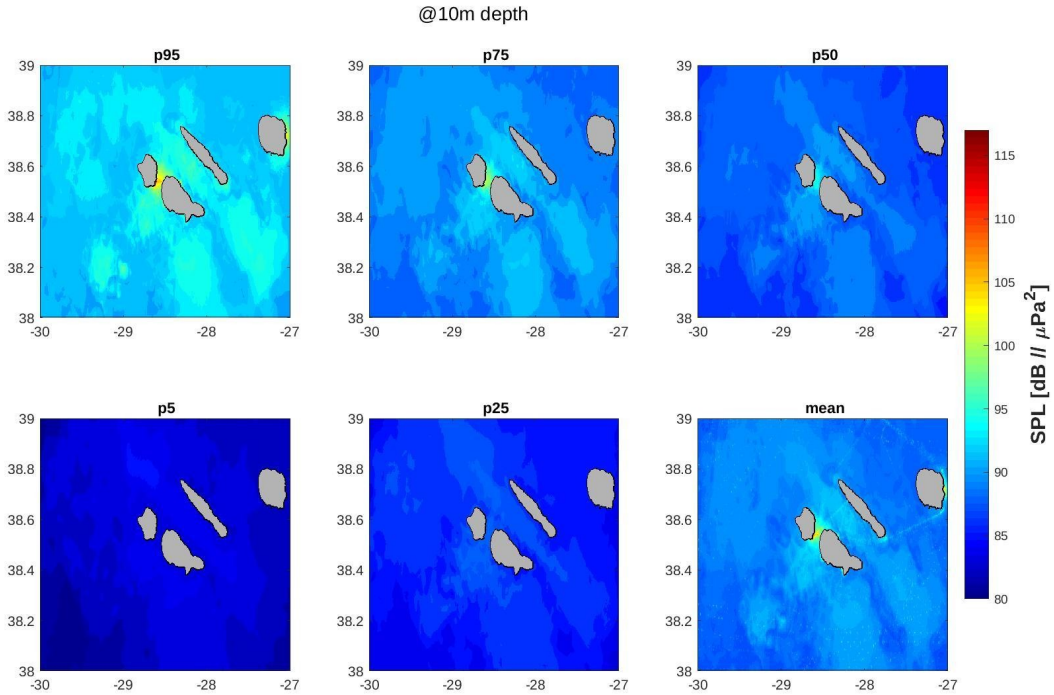

Figure 6.2.15: Field calibrated broadband modeled field: 5, 25, 50, 75 and 95% percentiles and time mean at 10 m depth in 40-1000 Hz, June 2018, 10 min average.

As mentioned above the effect of the calibration was to reduce the effective spread of the field and the overall levels in the lower portion of the frequency band. Although the overall mean levels seem in line and coherent with the known traffic routes and areas of shipping noise influence, whether that narrowing of variability with direct impact in the statistics is justified remains questionable and extremely hard to validate.

6.2.8. Azores case study conclusions

Because of the area covered in the JONAS project, it was not possible to perform calibration of the noise maps. In this document, the comparisons between measured and simulated noise levels are performed in order to provide confidence maps. The methodology is explained and two case studies are provided in the annexes. A one-month data set obtained in three evenly spaced recorders from IMAR-Okeanos group were used as a sample for calibration of a wide oceanic area containing four islands. Shipping routes between islands and in long routes across the area, as well as fishing traffic has been measured through AIS, together with surface wind generated noise were used for shipping noise modeling. Model output was compared to the measured data at the receiver locations, and statistical differences drawn. These differences were then applied to the whole data set for the whole area, to obtain a flavor of the field calibrated data set. Whether that calibrated mean surface may be deemed as closer to the truth surface is hard to tell. Validation would certainly require further validation points and / or comparison with other calibration methods among those proposed.

Acknowledgments

The Azores test case was done with the support of Mónica Silva, Irma Cascão and Miriam Romagosa from IMAR-Okeano, University of Azores, that provided the acoustic data of the three recorders near the Islands of Pico and Faial, and participated in many discussions and suggestions that were incorporated in the document. Cristiano Soares from Marsensing provided the AIS data and the shipping noise predictions for the whole Azores area. SMJ would like to personally thank them for their contribution, without which this work would not have been possible. DD and FLC would like to thank Hélène Pihan-Le-Bars, Benjamin Ollivier and Bazile Kinda from SHOM who provided the processed acoustic data in French waters (funded by the French Ministry of Ecological Transition). Authors would like to thank Evan Edwards and Denise Risch from MARPAMM project, Nathan Merchant and Rosalyn Putland from CEFAS as well as Arnaud Lefevre, Dominique Clorennec and Thomas Folegot from Quiet Ocean for providing acoustic data that were useful for the development of the methodologies but not included in this report.

References

[1] G. V Frisk, “Noiseonomics: The Relationship between Ambient Noise Levels in the Sea and Global Economic Trends,” vol. 2, no. (437).

[2] W. O. Knudsen, R. S. Alford, and J. W. Emling, “Underwater Ambient Noise,” vol. 7, pp. 410–429.

[3] G. . Wenz, “Acoustic Ambient Noise in the Ocean : Spectra and Sources,” *J. Acoust. Soc. Am.*, vol. 34, no. 12, pp. 1936–1956, 1962.

[4] R. J. Urick, *Principles of underwater sound*. New York, NY, 1983.

[5] D. H. Cato, “Ambient Sea Noise in Waters near Australia,” vol. 60, no. 2, pp. 320–328.

[6] A. S. Burgess and D. J. Kewley, “Wind-generated surface noise source levels in deep water east of Australia,” *J. Acoust. Soc. Am.*, vol. 73, no. 1, pp. 201–210, 1983.

[7] D. J. Kewley, D. G. Browning, and W. M. Carey, “Low-frequency wind-generated ambient noise source levels,” *J. Acoust. Soc. Am.*, vol. 88, no. 4, pp. 1894–1902, 1990.

[8] J. H. Wilson, “Wind-generated noise modeling,” *J. Acoust. Soc. Am.*, vol. 73, no. 1, pp. 211–216, 1983.

[9] M. J. Hinich, “Maximum-Likelihood Signal Processing for a Vertical Array,” vol. 54, no. 2, pp. 499–503.

[10] H. P. Bucker, “Use of Calculated Sound Fields and Matched-Detection to Locate Sound Sources in Shallow Water,” vol. 59, pp. 368–373.

[11] A. Tolstoy, *Matched Field Processing for Underwater Acoustics*. World Scientific.

[12] A. B. Baggeroer, W. Kuperman, and P. Mikhalevsky, “An Overview of Matched Field

Methods in Ocean Acoustics," vol. 18, no. 4, pp. 307–338.

[13] M. D. Collins and W. A. Kuperman, "Focalization: Environmental Focusing and Source Localization," vol. 90, no. 3, pp. 1410–1422.

[14] A. Tolstoy, O. Diachok, and N. L. Frazer, "Acoustic Tomography via Matched Field Processing," vol. 89, no. 3, pp. 1119–1127.

[15] E. K. Skarsoulis, Athanassoulis, and U. Send, "Ocean Acoustic Tomography Based on Peaks Arrivals," vol. 100, no. 2, pp. 797–813.

[16] O. C. Rodriguez and S. Jesus, "Physical Limitations of Travel-Time-Based Shallow Water Tomography," vol. 6, no. 108, pp. 2816–2822.

[17] Z.-H. Michalopoulou, "Robust Multi-Tonal Matched-Field Inversion: A Coherent Approach," vol. 104, pp. 163–170.

[18] S. M. Jesus, C. Soares, E. Coelho, and P. Picco, "An Experimental Demonstration of Blind Ocean Acoustic Tomography," vol. 119, no. 3, pp. 1420–1431.

[19] S. M. Jesus, C. Soares, and F. Zabel, "Shipping Noise Field Calibration via Source Inversion," in *IEEE MTS/OES Oceans 2017*.

[20] S. M. Kay, *Fundamentals of Statistical Signal Processing: Estimation Theory*, vol. 1. Prentice-Hall.

[21] G. B. C. G. 2020, "The GEBCO_2020 Grid - a Continuous Terrain Model of the Global Oceans and Land." British Oceanographic Data Centre, National Oceanography Centre, NERC, UK.

[22] M. O. Lammers, R. E. Brainard, W. W. L. Au, T. A. Mooney, and K. B. Wong, "An Ecological Acoustic Recorder (EAR) for Long-Term Monitoring of Biological and Anthropogenic Sounds on Coral Reefs and Other Marine Habitats," vol. 123, no. 3, pp. 1720–1728.

[23] C. Soares, F. Zabel, and S. M. Jesus, "A shipping noise prediction tool," in *MTS/IEEE OCEANS 2015 - Genova: Discovering Sustainable Ocean Energy for a New World*, 2015, no. February, pp. 1–7.

[24] M. F. McKenna, D. Ross, S. M. Wiggins, and J. A. Hildebrand, "Underwater Radiated Noise from Modern Merchant Ships," vol. 131, no. 1, pp. 92–103.

[25] C. Soares, A. Pacheco, F. Zabel, E. González-Goberña, and C. Sequeira, "Baseline Assessment of Underwater Noise in the Ria Formosa," vol. 150, p. 110731.

[26] C. Soares, R. Duarte, F. Zabel, M. A. Silva, and S. M. Jesus, "Shipping Noise Predictions from AIS in the Faial-Pico Area, Azores Archipelago," in *Global Oceans 2020: Singapore – U.S. Gulf Coast*, pp. 1–6.

[27] Folegot T., Clorennec D., Chavanne R., R. Gallou (2016). Mapping of ambient noise for BIAS. Quiet-Oceans technical report QO.20130203.01.RAP.001.01B, Brest, France, December 2016

[28] Le Courtois, F., Kinda, G. B., Boutonnier, J-M., Stéphan, Y., Sarzeaud, O. (2016). Statistical ambient noise maps from traffic at world and basin scales. In Acoustic and Environmental Variability, Fluctuations and Coherence, Cambridge, England.

[29] Ross, D., & Kuperman, W. A. (1989). Mechanics of underwater noise.

[30] Breeding Jr, J. E., Pflug, L. A., Bradley, M., & Walrod, M. H. (1996). Research Ambient Noise DIrectionality (RANDI) 3.1 Physics Description. Naval Research Lab Stennis Space Center MS.

[31] Wagstaff, R. A. (1973). RANDI: Research ambient noise directionality model. NAVAL UNDERSEA CENTER SAN DIEGO CA.

[32] Wales, S. C., & Heitmeyer, R. M. (2002). An ensemble source spectra model for merchant ship-radiated noise. The Journal of the Acoustical Society of America, 111(3), 1211-1231.

[33] Audoly, C., & Rizzuto, E. (2015). Ship underwater radiated noise patterns. AQUO European Collaborative., Project, Deliverable D, 2.

[34] Audoly, C., Gaggero, T., Baudin, E., Folegot, T., Rizzuto, E., Mullor, R. S., ... & Kellett, P. (2017). Mitigation of underwater radiated noise related to shipping and its impact on marine life: A practical approach developed in the scope of AQUO project. IEEE Journal of Oceanic Engineering, 42(2), 373-387.

[35] Wittekind, D. K. (2014). A simple model for the underwater noise source level of ships. Journal of Ship Production & Design, 30(1).

[36] Putland, R.L., Farcas, A., Merchant, N. D. (2021) Uncertainty assessment between measurements and model predictions for 2019 data. Final report. Report of the EU INTERREG Joint Monitoring Programme for Ambient Noise North Sea (Jomopans)

[36] Jousselme, A. L., & Maupin, P. (2012). Distances in evidence theory: Comprehensive survey and generalizations. International Journal of Approximate Reasoning, 53(2), 118-145.

[37] QUIETMED group, (2018). Deliverable D3.3 - Best practice guidelines on acoustic modelling and mapping. Joint programme on noise (D11) for the implementation of the Second Cycle of the MSFD in the Mediterranean Sea.

[38] Ainslie, M.A., Harrison, C.H. and Zampolli M. (2011) An analytical solution for signal, background and signal to background ratio for a low frequency active sonar in a Pekeris waveguide satisfying Lambert's rule. Proc. 4th International Conference and Exhibition on "Underwater Acoustic Measurements: Technologies & Results".

[39] Audoly, C., Rousset, C., Rizzuto, E., Mullor, R. S., Hallander, J., & Baudin, E. (2015, May). Mitigation measures for controlling the ship underwater radiated noise, in the scope of AQUO Project. In OCEANS 2015-Genova (pp. 1-6). IEEE.

[40] de Jong, CAF, Binnerts, B, Robinson, S, Wang, L (2021) Guidelines for modelling ocean ambient noise. Report of the EU INTERREG Joint Monitoring Programme for Ambient Noise North Sea (JOMOPANS).

[41] Dekeling, R. P. A., et al. "Monitoring Guidance for Underwater Noise in European Seas, Part II: Monitoring Guidance Specifications. A guidance document within the Common Implementation Strategy for the Marine Strategy Framework Directive by MSFD Technical Subgroup on Underwater Noise." (2014).

[42] Ji-Xun Zhou, Xue-Zhen Zhang & D. P. Knobles (2009) Low-frequency geoacoustic model for the effective properties of sandy seabottoms, J. Acoust. Soc. Am. 125(5), 2847–2866

[43] Taroudakis, M.I., Skarsoulis, E.K., Papadakis, P., Piperakis, G., Maglio, A., Drira, A., Gervaise, C., Le Courtois, F., 2018. Best practice guidelines on acoustic modelling and mapping (Deliverable 3.3). No. 11.0661/2016/748066/SUB/ENV.C2.

[43] Cha, S. H. (2007). Comprehensive survey on distance/similarity measures between probability density functions. City, 1(2), 1.

Annexe 1: Data fields for model setup

A1.1 Azores water column data

The Azores high pressure system is the weather engine for most of the north Atlantic and sets a relatively mild climate, with low winds and relatively warm water. In order to get a grasp of the spatial and time variability of water column temperature, Figure. A.1.1 shows the spatial location of mean temperature profiles over the area bathymetry (a), and water temperature variation in space in the top plots and bottom left, and the variation through time at one single location (bottom right) (b).

(a)

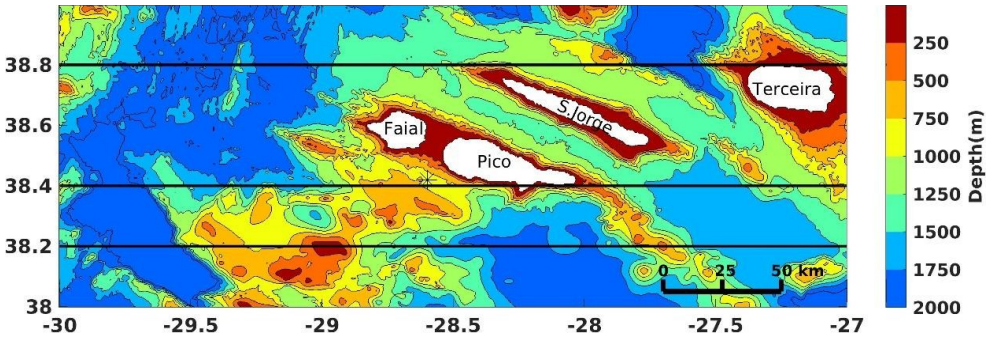

(b)

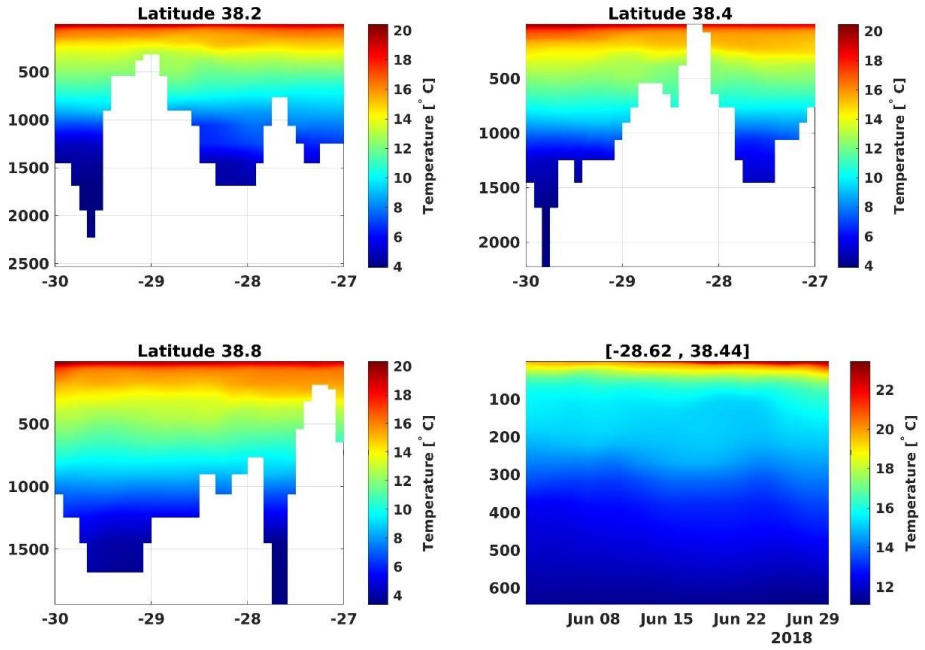

Figure A.1.1: Temperature, salinity and sound velocity profiles variation along the Azores area for the month of June 2018. Source: CMEMS-Copernicus Marine Service.

Clearly, temperature variation is very smooth along these longitude tracks crossing the whole observation area. In time we notice that an upper gradient is developing along the month of June.

Figure A.1.2 shows temperature, salinity and sound velocity profiles variability across the whole area and for the month of June 2018. This data was extracted from the CMEMS-Copernicus Marine Service[6] database. The water column shows a typical downward refracting sound velocity profile with a deep sound channel and where the critical depth is never attained. Variability is mild.

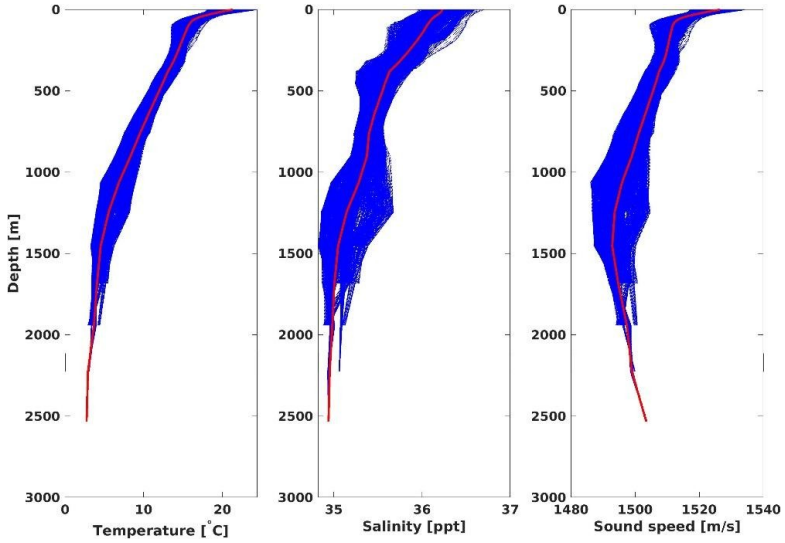

Figure A.1.2: Temperature, salinity and sound velocity profiles variation along the Azores area for the month of June 2018. Source: CMEMS-Copernicus Marine Service.

6 www.copernicus.eu

A1.2 Azores water column data

The cumulative ship distribution drawn from AISHub[7] over the whole month of June 2018 for the area at hand is given in Figure A.1.3 using logarithm base 10 of ship density evaluated in ship x hour per arc minute^2.

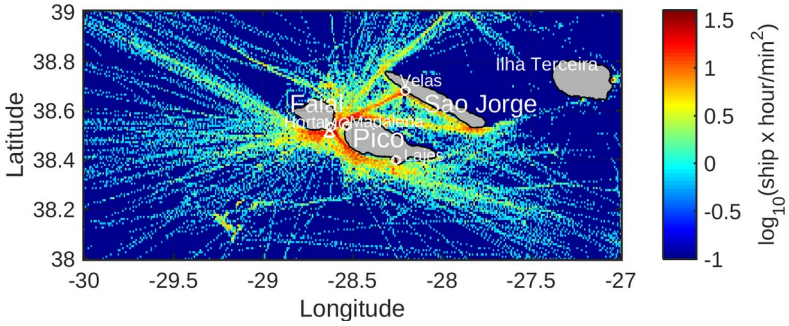

Figure A.1.3: Cumulative ship density for the month of June 2018 according to AISHub.

In reality this figure does not show the whole picture since it melts all the shipping contacts as simple dots. Since ship types and position in time and space are the primary input to the modeling effort, it is of paramount importance to have a better understanding of the AIS data set. That is why the data was sorted along various parameters pertinent to the data set, such as, speed, ship type, time and space. It was found, for instance, that approximately 25% of the contacts were ships in port or on anchor (speed zero), so these were discarded. The remaining contacts were sorted by type, using the ID tag existing in the AIS data stream. It was found that for approximately 50% of the remaining contacts ship type was not available. The other 50% were divided among: fishing, dredging, sailing, rescue, passenger, cargo, tanker and "other type" not classified in any of the previous. All in all, 600 different ships were recorded, producing about 60.000 contacts during one month. Different patterns were obtained when these ship types were separated along time (time of the day and day of the month). For instance, fishing was constant throughout day time while passenger and sailing were active only during day time, while the former had peaks around noon and then at the end of the day. Cargo was mostly active during night time and rescue only during the day. The group that could not be identified had an activity distribution very similar to sailing. Spatial distribution of the different ship types was also quite characteristic, with sailing covering long routes and around the islands, cargo and tankers well away from the islands (long routes), passenger linking ports only and fishing covering well known fishing spots.

A1.3 Azores wind speed forecast

Figure A.1.5 shows the the mean wind speed over the whole month of June 2018 as predicted by the ECMWF[8] with a resolution of 0.75×0.75 arc degree and 3-hour resolution.

7 ship Automatic Identification System data exchange, www.aishub.net

8 ship Automatic Identification System data exchange, www.aishub.net

European Centre for Medium-Range Weather Forecasts, www.ecmwf.int

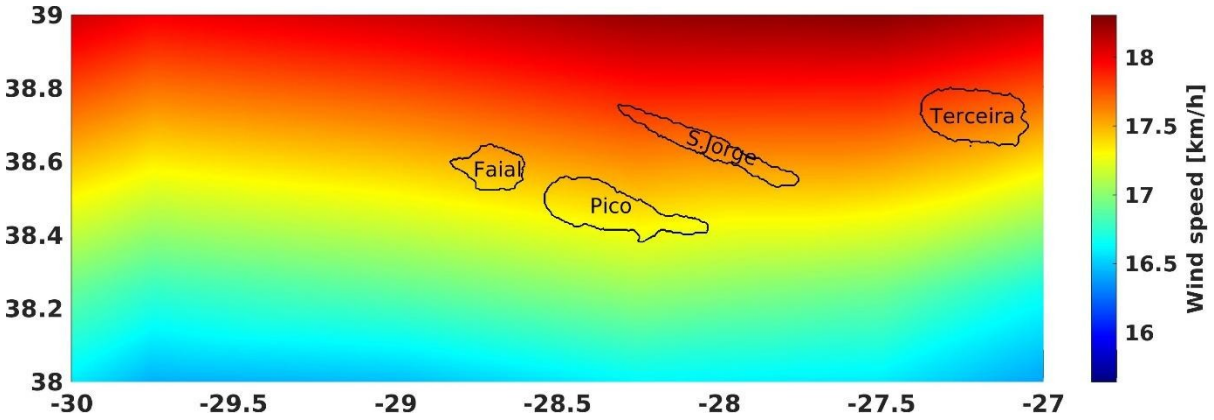

Figure A.1.5: Azores mean wind speed for June 2018, according to the ECMFW.